A reduced basis finite element heterogeneous multiscale method for Stokes flow in porous media

Assyr Abdulle* Ondrej Budáč*

Abstract

A reduced basis Darcy-Stokes finite element heterogeneous multiscale method (RB-DS-FE-HMM) is proposed for the Stokes problem in porous media. The multiscale method is based on the Darcy-Stokes finite element heterogeneous multiscale method (DS-FE-HMM) introduced in [A. Abdulle, O. Budáč, Multiscale Model. Simul. 13 (2015)] that couples a Darcy equation solved on a macroscopic mesh, with missing permeability data extracted from the solutions of Stokes micro problems at each macroscopic quadrature point. To overcome the increasingly growing cost of repeatedly solving the Stokes micro problems as the macroscopic mesh is refined, we parametrize the microscopic solid geometry and approximate the infinite-dimensional manifold of parameter dependent solutions of Stokes problems by a low-dimensional space. This low-dimensional (reduced basis) space is obtained in an offline stage by a greedy algorithm and used in an online stage to compute the effective Darcy permeability at a cost independent of the microscopic mesh. The discretization of the parametrized Stokes problems relies on a Petrov-Galerkin formulation that allows for a stable and fast online evaluation of the required permeabilities. A priori and a posteriori estimates of the RB-DS-FE-HMM are derived and a residual-based adaptive algorithm is proposed. Two- and three-dimensional numerical experiments confirm the accuracy of the RB-DS-FE-HMM and illustrate the speedup compared to the DS-FE-HMM.

Keywords. Stokes flow, Darcy equation, numerical homogenization, reduced basis, adaptivity

AMS subject classifications. 65N30, 76D07, 74Qxx, 35Q86

1 Introduction

Fluid flow in porous media is an important process that is present in many scientific and engineering applications. It is usually described by an effective flow equation, the well-known Darcy equation, that describes a porous medium as a homogeneous domain whose porosity is taken into account in a macroscopic parameter, the effective permeability. For some applications, the effective permeability can be obtained experimentally or computed form micro-scale Darcy equations. Sometimes, however, computations or experiments at pore scales are required. One has then to switch to another description of the fluid flow, namely Stokes or Navier-Stokes equations. Fluid flow in porous medium typically exhibits slow motion and inertial terms can be neglected, hence, the Stokes equation is often a good description of the physical process at pore scales. Yet numerical simulations of the Stokes equations at the pore scale denoted by ε in what follows (typically micrometer scale), over a computational domain ranging from lab scale (centimeter) to field scale (meter) lead to a number of degrees of freedom often impossible to handle even on modern supercomputers. Such problems thus require multiscale methods combining pore scale computations on small sampling domains of the computational domain with a macroscopic effective computation. Such numerical methods are often based on the mathematical homogenization theory that we briefly describe.

*ANMC, Mathematics Section, École Polytechnique Fédérale de Lausanne, CH-1015 Lausanne, Switzerland, {assyr.adulle,ondrej.budac epfl.ch}

Homogenization of fluid flow in porous media is the mathematical description of the asymptotic behavior of the flow when $\varepsilon \to 0$. This mathematical theory for the Stokes equation in periodic porous domain was first described in [40] using arguments based on asymptotic expansion. It was shown that the macroscopic description is the Darcy equation and that the macroscopic permeability can be computed from a microscopic computation using the Stokes equation in a sampling domain taking into account the pore geometry. These findings were rigorously establish by Tartar [42] and generalized by Allaire [9]. Further works include the analysis of correctors [28], the description of stochastically homogeneous media [14], etc. Homogenization theory has triggered the development of numerical techniques that rely on the effective Darcy equation but recover the permeability using information about the porous structure. Since effective permeability is a local property, these methods can avoid resolving the full fine scale details in the whole medium.

Here we focus on methods that are based on the *heterogeneous multiscale method* (HMM), reviewed in [5]. The HMM framework was successfully applied to the Stokes problem in the *Darcy-Stokes finite element heterogeneous multiscale method* (DS-FE-HMM) introduced in [2]. The DS-FE-HMM is based on the Darcy-Stokes coupling described by the homogenization theory. The *finite element method* (FEM) with numerical quadrature is used to discretize the macroscopic Darcy problem. Around each macroscopic quadrature point, a sampling domain is considered where the local porous structure is discretized by a microscopic mesh. Based on this mesh, the pore scale Stokes equation is then computed using a (micro) FEM. The micro solutions then provide an approximation of the local effective permeability at the macroscopic quadrature points. As macro and micro meshes need to be refined simultaneously to avoid error saturation, an adaptive algorithm based on an a posteriori error analysis for the DS-FE-HMM has been developed in [2]. Precisely, adaptive refinement of both the macro Darcy problem and the micro Stokes problems was proposed and shown to speedup considerably the multiscale algorithm compared to mesh refinement based on a priori error analysis. Other adaptive algorithms for the HMM focusing only on the macroscopic elliptic problem can be found in [1, 2, 7, 32]. Other numerical method that rely on the Stokes equation at pore scale have been proposed in [2, 10, 18, 41]. The multiscale approach in [10] uses the control volume method to discretize the Darcy equation, while the multiscale FEM [18] uses a hierarchy of macroscopic grids where micro problems are solved with various accuracy.

Due to the large number of micro Stokes problems that need to be computed with increased precision (d problems at each macroscopic quadrature point in $\mathbb{R}^d$), the DS-FE-HMM can be still computationally expensive, especially for three-dimensional problems or if high precision is required. Departing from the the described micro-macro strategy, the idea is to use the possible similarity of the family of the micro problems. In this paper we combine a model order reduction techniques with the DS-FE-HMM that reduce significantly the computational cost of the plain DS-FE-HMM, while maintaining the general applicability of this method, namely the variation of the micro structure does not have to be smooth and domains (macroscopic and microscopic) can have arbitrary (non-convex) shapes. Our new method relies on the reduced basis (RB) method to efficiently solve the Stokes micro problems and is called the reduced basis Darcy-Stokes finite element heterogeneous multiscale method (RB-DS-FE-HMM). As in the DS-FE-HMM, the new algorithm is based on FEM with numerical quadrature to solve the Darcy problem on a macroscopic mesh. To obtain the permeabilities, we perform computation in a reduced basis space of representative Stokes solution in the following way. We assume that the local porous structure at any point of the macroscopic domain can be obtained from a reference micro domain by a known map. Hence, the Stokes micro problems can be pulled back to a reference domain, where they become saddle-point problems with varying coefficients. This reformulation allows us to define a single reference micro mesh that is used for the discretization of all micro problems. The model order reduction algorithm for the Darcy-Stokes problem is then divided into two stages:

- The *offline* stage that can be computationally expensive but is executed only once. A small number of representative microscopic geometries (sampling domains in the macroscopic domain) are selected, for which the corresponding Stokes micro problems are solved accurately on a reference micro mesh. The collection of Stokes solutions at the selected points span the reduced basis space.
- The *online* stage is a fast procedure that efficiently computes an accurate approximation of the effective permeability for any quadrature point in the macroscopic domain using

the precomputed (micro mesh independent) reduced basis space. As the reduced basis space is usually of low dimension and independent of the macroscopic mesh, these latter computations are usually very fast.

The reduced basis method has been applied to the (single scale) Stokes problem in parametrized geometry by several authors. In [24, 37, 39], a saddle-point formulation is used. When combined with the reduced basis strategy, there are two issues that must be addressed, namely the approximation stability (non-degeneracy of the Brezzi inf-sup condition) and the algebraic stability (bounded condition number of the reduced system). It is shown in [24, 37, 39] that by enriching appropriately the pressure space both requirements can be fulfilled. The resulting method can, however, be expensive in the online stage. Alternative methods with smaller online systems can be constructed but its stability can no longer be guaranteed (see [4] for a more detailed description). On the other hand, there are RB methods that study parametrized linear non-coercive problems, see [4, 22, 27, 36] and the references therein. They have no assumptions on the structure of the problem and use only the Babuška inf-sup condition as a stability indicator. This is the chosen framework to develop the reduced basis strategy for our multiscale problem and we consider a Petrov–Galerkin RB method with a fixed solution space and a parameter-dependent test space that was first introduced in [36] and was recently derived for the Stokes problem in [4]. Another advantage of this formulation is its flexibility to enforce additional Lagrange multipliers as used in our formulation to normalize pressure. We derive a fully-discrete a priori error analysis of the RB-DS-FE-HMM that reveals the contribution to the error of the various approximation steps: the microscopic error (due to the FEM used to compute the RB functions), the RB error, and the macroscopic error. We also provide an adaptive strategy for our new method and derive related a posteriori error estimates.

This paper is organized as follows. We define different types of porous media and the model problem in section 2. A short review of the DS-FE-HMM in given in section 3. The RB-DS-FE-HMM is explained sections 4 and 5. While the parametrization of the geometry and the overall multiscale algorithm combining the reduced basis method with the Stokes to Darcy approximation is detailed in section 4 we show in section 5 how the greedy construction of the RB is performed and we detail the computation of rigorous a posteriori error estimates, including the inf-sup stability constants. A priori and a posteriori error estimates are considered in section 6 and an adaptive method is proposed in section 7. Finally, numerical examples for two and three dimensional problems illustrating the theoretical estimates and the performance of the method are presented in section 8.

1.1. Notation. Let C denote a generic constant whose value can change at any occurrence but it depends only on explicitly indicated quantities. We consider a domain $\Omega \subset \mathbb{R}^d$, $d \in \mathbb{N}$ and the usual Lebesgue space $L^p(\Omega)$ and Sobolev space $W^{k,p}(\Omega)$ equipped with the usual norms $\|\cdot\|_{L^p(\Omega)}$ and $\|\cdot\|_{W^{k,p}(\Omega)}$. On the factor space $L^2(\Omega)/\mathbb{R}$, we define $\|q\|_{L^2(\Omega)/\mathbb{R}} = \inf_{s\in\mathbb{R}} \|q+s\|_{L^2(\Omega)}$. For $p=2$ we apply the Hilbert space notation $H^k(\Omega)$ and $H^1_0(\Omega)$ and define the seminorm $|q|_{H^1(\Omega)} = (\sum_{i=1}^d \|\partial_i q\|^2_{L^2(\Omega)})^{1/2}$. The standard scalar product on $L^2(\Omega)$ is denoted by $(\cdot,\cdot)_{L^2(\Omega)}$. Given a matrix $A \in \mathbb{R}^{d\times d}$ with entries A_{ij}, we denote its Frobenius norm by $\|A\|_{\mathrm{F}} = (\sum_{i,j=1}^d A_{ij}^2)^{1/2}$. Given a vector $\xi \in \mathbb{R}^d$ with entries ξ_i, we define $|\xi| = (\sum_{i=1}^d \xi_i^2)^{1/2}$.

2 Problem setting and homogenization

Let $d \in \{2,3\}$ and $\Omega \subset \mathbb{R}^d$ be a bounded, connected domain. We consider a porous structure in Ω by dividing Ω into a fluid part $\Omega_\varepsilon \subset \Omega$ and a solid part $\Omega\backslash\Omega_\varepsilon$, where $\varepsilon > 0$ indicates the size of the pore scale. Fluid flow in Ω_ε can be modeled by the Stokes equation

$$\begin{aligned} -\Delta \mathbf{u}^\varepsilon + \nabla p^\varepsilon &= \mathbf{f} \quad \text{in } \Omega_\varepsilon, \\ \operatorname{div} \mathbf{u}^\varepsilon &= 0 \quad \text{in } \Omega_\varepsilon, \\ \mathbf{u}^\varepsilon &= 0 \quad \text{on } \partial\Omega_\varepsilon \end{aligned} \tag{1}$$

with a given force field $\mathbf{f}$, an unknown velocity field $\mathbf{u}^\varepsilon$ and pressure p^ε. Solving (1) with mesh-based techniques requires meshsize $h < \varepsilon$, which can be computationally prohibitive for $\varepsilon \ll \operatorname{diam}(\Omega)$. Efficient models and numerical methods that approximate (1) rely on an

effective equation, e.g., the Darcy law.

Homogenization theory for the Stokes problem [9, 28, 29, 40, 42] studies the limit behavior of the solutions of (1) for $\varepsilon \to 0^+$ under the assumption that Ω_ε is a periodic porous domain (see section 2.1). The pore geometry that is periodically repeated in Ω_ε determines the homogenized permeability tensor $a^0 \in \mathbb{R}^{d\times d}$ such that the following limit property is true. The pressure solution p^ε of (1), defined in Ω_ε, can be extended to P^ε, defined in Ω, such that P^ε converges strongly to p^0 in $L^2_{\mathrm{loc}}(\Omega)/\mathbb{R}$, where p^0 is the homogenized pressure that is given as a solution to the Darcy equation

$$\begin{aligned} \nabla \cdot a^0(\mathbf{f} - \nabla p^0) &= 0 \quad \text{in } \Omega, \\ a^0(\mathbf{f} - \nabla p^0) \cdot \mathbf{n} &= 0 \quad \text{on } \partial\Omega. \end{aligned} \tag{2}$$

Furthermore, the velocity solution $\mathbf{u}^\varepsilon$ of (1) can be extended to $\mathbf{U}^\varepsilon$, defined in Ω, such that $\mathbf{U}^\varepsilon/\varepsilon^2$ converges to $\mathbf{u}^0$ weakly in $L^2(\Omega)^d$, where the homogenized velocity $\mathbf{u}^0$ satisfies $\mathbf{u}^0 = a^0(\mathbf{f} - \nabla p^0)$. Homogenization theory is less developed for non-periodic media, i.e., when the solid part can vary locally [2, 14, 18]. In this situation a^0 in (2) can depend on $x \in \Omega$.

We continue with a brief description of periodic and locally periodic porous media. For a comparison of the two see Figure 1.

2.1. Periodic porous media. We recall the definition of Ω_ε from [9]. We denote by Y the d-dimensional unit cube $(-1/2, 1/2)^d$. Let $Y_{\mathrm{S}} \subset \overline{Y}$ and set $Y_{\mathrm{F}} = Y \backslash Y_{\mathrm{S}}$. Here and subsequently, the subscripts F and S stand for the fluid and solid part, respectively. Let $\varepsilon > 0$ and define

$$\Omega_\varepsilon = \Omega \backslash \bigcup_{x \in (1/2+\mathbb{Z})^d} \varepsilon(x + Y_{\mathrm{S}}). \tag{3}$$

It is further assumed in [9] that the set Y_{S} is closed in $\overline{Y}$, and both Y_{S} and Y_{F} have positive measure. Moreover, the sets Y_{F} and $\mathbb{R}^d \backslash \cup_{x\in\mathbb{Z}^d} (x + Y_{\mathrm{S}})$ are connected, have locally Lipschitz boundaries, and are locally located on one side of their boundaries.

2.2. Locally periodic porous media. We consider a generalization of periodic porous media as presented in [2]. Let $\varphi : \mathbb{R}^d \times \overline{Y} \to \overline{Y}$ be a continuous map and assume that $\varphi(x, \cdot) : \overline{Y} \to \overline{Y}$ is a homeomorphism such that $\varphi(x, \cdot)$ and $\varphi^{-1}(x, \cdot)$ are in $W^{1,\infty}(Y)$ for every $x \in \mathbb{R}^d$. For $\varepsilon > 0$ define

$$\Omega_\varepsilon = \Omega \backslash \bigcup_{x \in (1/2+\mathbb{Z})^d} \varepsilon(x + \varphi(\varepsilon x, Y_{\mathrm{S}})). \tag{4}$$

The *reference pore geometry* $(Y_{\mathrm{S}}, Y_{\mathrm{F}})$ is thus mapped via φ to the *local pore geometries* $Y^x_{\mathrm{S}} = \varphi(x, Y_{\mathrm{S}})$ and $Y^x_{\mathrm{F}} = Y \backslash Y^x_{\mathrm{S}}$. If $\varphi(x, y) \equiv y$ then the definitions (3) and (4) are equivalent.

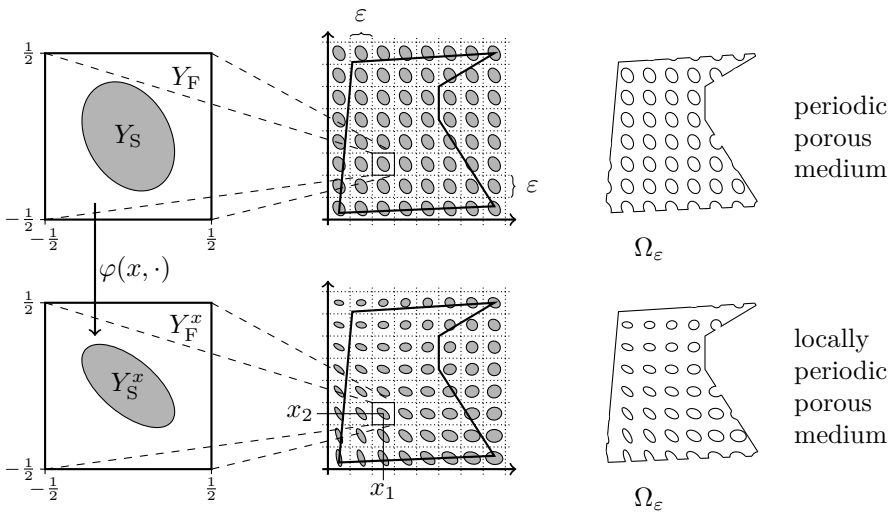

Figure 1: A comparison of periodic (above) and locally periodic (below) porous media.

2.3. Model problem. Formal homogenization of the Stokes problem (1) in locally periodic porous media gives the effective equation (2), however, the permeability $a^0 : \Omega \to \mathbb{R}^{d\times d}$ now depends on the local pore geometries $(Y_{\mathrm{F}}^x,\, Y_{\mathrm{S}}^x)$. Consider the velocity space

$$W(Y_{\mathrm{F}}^x) = \{\mathbf{v} \in H^1(Y_{\mathrm{F}}^x)^d;\ \mathbf{v} = 0 \text{ on } \partial Y_{\mathrm{S}}^x, \mathbf{v} \text{ is } Y\text{-periodic}\}.$$

For a given $x \in \Omega$ and for every $i \in \{1, \dots, d\}$ we solve the Stokes micro problem: Find $\mathbf{u}^{i,x} \in W(Y_{\mathrm{F}}^x)$ and $p^{i,x} \in L^2(Y_{\mathrm{F}}^x)/\mathbb{R}$ such that

$$\begin{aligned} a(\mathbf{u}^{i,x}, \mathbf{v}) + b(\mathbf{v}, p^{i,x}) &= g^i(\mathbf{v}) && \forall \mathbf{v} \in W(Y_{\mathrm{F}}^x), \\ b(\mathbf{u}^{i,x}, q) &= 0 && \forall q \in L^2(Y_{\mathrm{F}}^x)/\mathbb{R}, \end{aligned} \tag{5}$$

where

$$a(\mathbf{u}, \mathbf{v}) = \sum_{i=1}^{d} \int_{Y_{\mathrm{F}}^x} \frac{\partial \mathbf{u}}{\partial y_i} \cdot \frac{\partial \mathbf{v}}{\partial y_i}\, \mathrm{d}y, \qquad g^i(\mathbf{v}) = \int_{Y_{\mathrm{F}}^x} \mathbf{v}_i\, \mathrm{d}y,$$

$$b(\mathbf{v}, q) = -\sum_{i=1}^{d} \int_{Y_{\mathrm{F}}^x} q \frac{\partial \mathbf{v}_i}{\partial y_i}\, \mathrm{d}y.$$

Then we have $a^0(x) = \int_{Y_{\mathrm{F}}^x} [\mathbf{u}^{1,x}, \mathbf{u}^{2,x}, \dots, \mathbf{u}^{d,x}]\, \mathrm{d}y$, or component-wise

$$a_{ij}^0(x) = \int_{Y_{\mathrm{F}}^x} \mathbf{u}_i^{j,x}\, \mathrm{d}y = g^i(\mathbf{u}^{j,x}) \qquad \forall i, j \in \{1, \dots, d\}. \tag{6}$$

Even for very simple micro geometries $(Y_{\mathrm{F}}^x, Y_{\mathrm{S}}^x)$ the tensor $a^0(x)$ is not known explicitly and we can only approximate it numerically.

Well-posedness of the model problem. It can be shown (see [40]) that $a^0(x)$ is symmetric and positive definite for every $x \in \Omega$. However, the *uniform ellipticity and boundedness* of $a^0(x)$ is more subtle as is examined thoroughly in [2]. The well-posedness of the micro problems (5) is guaranteed by an inf-sup condition (written here in the sense of Brezzi, see [17])

$$\beta_{\mathrm{Br}}(x) := \inf_{q \in L^2(Y_{\mathrm{F}}^x)/\mathbb{R}} \sup_{\mathbf{v} \in W(Y_{\mathrm{F}}^x)} \frac{b(\mathbf{v}, q)}{|\mathbf{v}|_{H^1(Y_{\mathrm{F}}^x)} \|q\|_{L^2(Y_{\mathrm{F}}^x)/\mathbb{R}}} > 0. \tag{7}$$

Lagrange multiplier formulation. Considering numerical approximation of (5), the quotient space $L^2(Y_{\mathrm{F}}^x)/\mathbb{R}$ can be resolved by one of the standard strategies:

- fix one degree of freedom of the pressure and normalize it afterward.
- use an iterative numerical method that does not assume that the system matrix is regular and takes care of the normalization (e.g., the Uzawa method [33]).
- use Lagrange multipliers to enforce the average of the pressure to be zero.

While all three are applicable for solving a single problem, the third one is convenient when combined with the reduced basis method as we will see in section 4. The system (5) with Lagrange multipliers that is written as single equation reads: Find $\mathbf{u}^{i,x} \in W(Y_{\mathrm{F}}^x)$, $p^{i,x} \in L^2(Y_{\mathrm{F}}^x)$, and $\lambda^{i,x} \in \mathbb{R}$ such that

$$a(\mathbf{u}^{i,x}, \mathbf{v}) + b(\mathbf{v}, p^{i,x}) + b(\mathbf{u}^{i,x}, q) + c(q, \lambda^{i,x}) + c(p^{i,x}, \kappa) = g^i(\mathbf{v}) \tag{8}$$

for every $\mathbf{v} \in W(Y_{\mathrm{F}}^x)$, $q \in L^2(Y_{\mathrm{F}}^x)$, and $\kappa \in \mathbb{R}$, where $c(q, \kappa) = \kappa \int_{Y_{\mathrm{F}}^x} q\, \mathrm{d}y$. The problem (8) will be later mapped into a reference domain Y_{F} and written compactly as a non-coercive problem in the space $X = W(Y_{\mathrm{F}}) \times L^2(Y_{\mathrm{F}}) \times \mathbb{R}$ in (20).

3 The DS-FE-HMM

In this section we briefly introduce the *Darcy-Stokes finite element heterogeneous multiscale method* [2,3] for solving the problem (2), (6), (5). Let $\varepsilon > 0$ and assume that Ω and Ω_ε are connected bounded polygonal domains in $\mathbb{R}^d$ with $\Omega_\varepsilon \subset \Omega$. We recall that this numerical method does not require Ω_ε to be periodic nor locally periodic.

Macro FE space and quadrature formulas. Let $\{\mathcal{T}_H\}$ be a family of conformal, shape-regular triangulations of Ω parametrized by the mesh size $H = \max_{K\in\mathcal{T}_H} H_K$, where $H_K = \operatorname{diam}(K)$. We consider the macro FE space

$$S^l_H(\Omega) = \{q^H \in H^1(\Omega);\ q^H|_K \in \mathcal{P}^l(K),\ \forall K \in \mathcal{T}_H\},$$

where $\mathcal{P}^l(K)$ is the space of polynomials on K of degree $l \in \mathbb{N}$. For each element $K \in \mathcal{T}_H$ we consider a quadrature formula $(x_{K_j}, \omega_{K_j})_{j=1,\dots,J}$ with integration points x_{K_j} and weights ω_{K_j}. Well-posedness of the DS-FE-HMM and the optimal order of accuracy rely on the following assumption on the quadrature formula [21, Chap. 4.1], which is satisfied, e.g., for $l = 1$, $J = 1$, $\omega_{K_1} = |K|$, and x_{K_1} as the barycenter of K.

Assumption (Q). We assume that $\int_{\hat{K}} \hat{q}(\hat{x})\,\mathrm{d}\hat{x} = \sum_{j=1}^J \hat{\omega}_j \hat{q}(\hat{x}_j)$ for any $\hat{q}(\hat{x}) \in \mathcal{P}^m(\hat{K})$, where $m = \max(2l-2, l)$.

Micro FE spaces. Let $\delta \geq \varepsilon$. For each quadrature point $x \in \Omega$ we define the micro sampling domain around x by

$$Y_{\mathrm{S}}^{x,\delta} = (((\mathbb{R}^d \backslash \Omega_\varepsilon) \cap (x + \delta\overline{Y})) - x)/\varepsilon, \qquad Y_{\mathrm{F}}^{x,\delta} = ((\delta/\varepsilon)Y)\backslash Y_{\mathrm{S}}^{x,\delta}. \tag{9}$$

Let $\{\mathcal{T}_h^x\}$ be a family of conformal, shape-regular triangulations of $Y_{\mathrm{F}}^{x,\delta}$ parametrized by the mesh size $h = \max_{T\in\mathcal{T}_h^x} h_T$, where $h_T = \operatorname{diam}(T)$. The shape-regularity constants are assumed to be the same for each quadrature point $x \in \Omega$ and $\delta \geq \varepsilon$. We consider the Taylor-Hood $\mathcal{P}^{k+1}/\mathcal{P}^k$ finite elements for $k \geq 1$, see [16]. The pressure and velocity FE spaces are given by

$$\begin{aligned} L_h(Y_{\mathrm{F}}^{x,\delta}) &= \{q \in S_h^k(Y_{\mathrm{F}}^{x,\delta});\qquad q \text{ is } (\delta/\varepsilon)Y\text{-periodic}\},\\ W_h(Y_{\mathrm{F}}^{x,\delta}) &= \{\mathbf{v} \in S_h^{k+1}(Y_{\mathrm{F}}^{x,\delta})^d;\quad \mathbf{v} \text{ is } (\delta/\varepsilon)Y\text{-periodic},\quad \mathbf{v} = 0 \text{ on } \partial Y_{\mathrm{S}}^{x,\delta}\}, \end{aligned} \tag{10}$$

respectively. We assume that the micro meshes $\mathcal{T}_h^x$ are conformal over periodic boundaries and periodicity can be thus enforced strongly.

Remark 1. The DS-FE-HMM can also work with other types of micro FEs (e.g., MINI) and different boundary conditions on ∂Y (e.g., Neumann).

DS-FE-HMM. The multiscale method is defined as follows: Find $p^H \in S^l_H(\Omega)/\mathbb{R}$ such that

$$B_H(p^H, q^H) = L_H(q^H) \qquad \forall q^H \in S^l_H(\Omega)/\mathbb{R}, \tag{11}$$

where the discrete macro bilinear form and right-hand side are given by

$$\begin{aligned} B_H(p^H, q^H) &= \sum_{K\in\mathcal{T}_H} \sum_{j=1}^J \omega_{K_j} a^h(x_{K_j}) \nabla p^H(x_{K_j}) \cdot \nabla q^H(x_{K_j}),\\ L_H(q^H) &= \sum_{K\in\mathcal{T}_H} \sum_{j=1}^J \omega_{K_j} a^h(x_{K_j}) \mathbf{f}^H(x_{K_j}) \cdot \nabla q^H(x_{K_j}). \end{aligned} \tag{12}$$

Here, $\mathbf{f}^H \in S^{l-1}_{\mathrm{dis},H}(\Omega)^d$ is an appropriate interpolation of the force field $\mathbf{f} \in L^2(\Omega)^d$, where

$$S^{l-1}_{\mathrm{dis},H}(\Omega) = \{q^H \in L^2(\Omega);\ q^H|_K \in \mathcal{P}^{l-1}(K),\ \forall K \in \mathcal{T}_H\}, \tag{13}$$

and $a^h(x_{K_j})$ is a numerical approximation of the tensor $a^0(x_{K_j})$ computed by the following micro Stokes problems. For each $i \in \{1, \dots, d\}$ and quadrature point $x \in \Omega$ we find $\mathbf{u}^{i,x,h} \in W_h(Y_{\mathrm{F}}^{x,\delta})$ and $p^{i,x,h} \in L_h(Y_{\mathrm{F}}^{x,\delta})/\mathbb{R}$ such that

$$\begin{aligned} a(\mathbf{u}^{i,x,h}, \mathbf{v}) + b(\mathbf{v}, p^{i,x,h}) &= g^i(\mathbf{v}) \qquad \forall \mathbf{v} \in W_h(Y_{\mathrm{F}}^{x,\delta})\\ b(\mathbf{u}^{i,x,h}, q) &= 0 \qquad \forall q \in L_h(Y_{\mathrm{F}}^{x,\delta})/\mathbb{R} \end{aligned} \tag{14}$$

and set $a^h(x) = \int_{Y_{\mathrm{F}}^{x,\delta}} [\mathbf{u}^{1,x,h}, \mathbf{u}^{2,x,h}, \dots, \mathbf{u}^{d,x,h}]\,\mathrm{d}y$, or equivalently $a^h_{ij}(x) = g^i(\mathbf{u}^{j,x,h})$ for every $i, j \in \{1, \dots, d\}$. An illustration of the coupling in DS-FE-HMM is given in Figure 2.

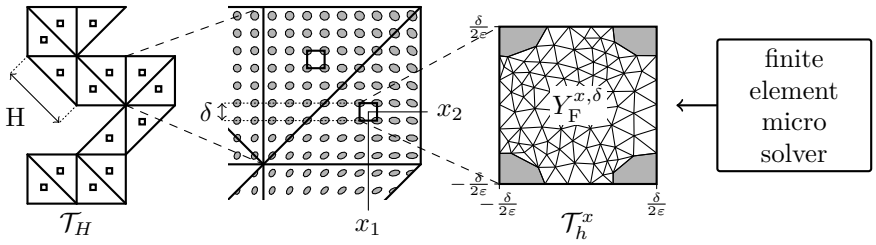

Figure 2: A sketch of the DS-FE-HMM.

Well-posedness of the DS-FE-HMM. For well-posedness of the macro problem (11) we require that $a^h(x)$ is uniformly elliptic and bounded over all macro quadrature points, which was studied in [2] and proved under rather generic assumptions on the geometries $Y_{\mathrm{F}}^{x,\delta}$.

3.1. A priori error estimates. We describe the a priori error analysis derived in [2]. One can use triangle inequality to decompose the error into three components:

$$|p^0 - p^H|_{H^1(\Omega)} \leq e_{\mathrm{mac}} + e_{\mathrm{mod}} + e_{\mathrm{mic}}. \tag{15}$$

The *macro error* e_{mac} arises from using the macro quadrature formula instead of exact integration. If $p^0 \in H^{l+1}(\Omega)$, Assumption **(Q)** holds, and $a^0(\cdot)$ is uniformly elliptic, bounded, and sufficiently smooth, then we have $e_{\mathrm{mac}} \leq CH^l$, where C is independent of H and ε.

The *modeling error* e_{mod} quantifies the non-optimal sampling of the micro structure (using $Y_{\mathrm{F}}^{x,\delta}$ instead of Y_{F}^{x}). Let us denote by Q^H the set of all macro quadrature points x_{K_j} and by $\overline{a}(x)$ the permeability computed with micro problems similar to (14) but solved in the Sobolev spaces. We then have $e_{\mathrm{mod}} \leq C\|\mathbf{f}^H\|_{L^2(\Omega)} \max_{x\in Q^H} \|a^0(x) - \overline{a}(x)\|_{\mathrm{F}}$. The constant C depends only on the ellipticity and boundedness constant of $a^0(x)$ and $\overline{a}(x)$.

The *micro error* e_{mic} arises from the approximation of the micro problems using the FEM and we have $e_{\mathrm{mic}} \leq C\|\mathbf{f}^H\|_{L^2(\Omega)} \max_{x\in Q^H} \|\overline{a}(x) - a^h(x)\|_{\mathrm{F}}$, where C depends only on the ellipticity and boundedness constant of $\overline{a}(x)$ and $a^h(x)$. If the micro solutions are sufficiently regular, one can obtain $e_{\mathrm{mic}} \leq Ch^{k+2}$. Notice that due to the rescaling in (9) the convergence rates depend on h and not h/ε, the usual scaling for the elliptic FE-HMM [1, 7]).

The optimal rates $e_{\mathrm{mac}} \leq CH^l$ and $e_{\mathrm{mic}} \leq Ch^{k+2}$ are normally not attained in practice, due to non-convexity of domains [2].

3.2. Computational cost. The computational cost of the DS-FE-HMM does not depend on the pore size ε but only on δ/ε, which is usually low. Denote the number of macroscopic *degrees of freedom* (DOF) by N_{mac} and the (average, per micro domain) number of microscopic DOF by N_{mic}. If the computational cost of solving one (micro or macro) problem is assumed to be linear in the DOF, the total cost of the DS-FE-HMM is $\mathcal{O}(N_{\mathrm{mic}}N_{\mathrm{mac}})$. To avoid saturation of error during refinement both N_{mic} and N_{mac} need to grow in a balanced way, leading to an optimal refinement relation $N_{\mathrm{mic}} \approx N_{\mathrm{mac}}^r$, where $r > 0$ depends on the type of the FE used and the regularity of the problem. Since uniform refinement is usually not optimal, an adaptive strategy was studied in [2, 3]. Even with adaptivity, computing a large amount of micro problems can be too expensive, especially for three-dimensional problems.

4 The RB-DS-FE-HMM

In this section we introduce a new method, the *reduced basis Darcy-Stokes finite element heterogeneous multiscale method* that addresses the high computational cost of the DS-FE-HMM on the micro scale. On the macro scale we solve a Darcy problem that is similar to (11) but a different tensor, denoted $a^{\mathrm{RB}}(x)$, is used. We apply a *reduced basis* (RB) method based on [4] to compute $a^{\mathrm{RB}}(x)$. The macroscopic equation reads: Find $p^{H,\mathrm{RB}} \in S_H^l(\Omega)/\mathbb{R}$ such that

$$B_H^{\mathrm{RB}}(p^{H,\mathrm{RB}}, q^H) = L_H^{\mathrm{RB}}(q^H) \qquad \forall q^H \in S_H^l(\Omega)/\mathbb{R}, \tag{16}$$

where

$$B_H^{\mathrm{RB}}(p^H, q^H) = \sum_{K\in\mathcal{T}_H}\sum_{j=1}^{J} \omega_{K_j} a^{\mathrm{RB}}(x_{K_j}) \nabla p^H(x_{K_j}) \cdot \nabla q^H(x_{K_j}),$$
$$L_H^{\mathrm{RB}}(q^H) = \sum_{K\in\mathcal{T}_H}\sum_{j=1}^{J} \omega_{K_j} a^{\mathrm{RB}}(x_{K_j}) \mathbf{f}^H(x_{K_j}) \cdot \nabla q^H(x_{K_j}). \tag{17}$$

For any quadrature point $x = x_{K_j}$ the tensor $a^{\mathrm{RB}}(x)$ is an approximation of $a^0(x)$ computed in the reduced basis space (see (29) and (33) below). An illustration of the RB-SD-FE-HMM is depicted in Figure 4.

Let us sketch here the RB method for computing a^{RB}. We assume that the Stokes micro problems can be mapped to a reference micro domain, where we obtain a parametric PDE. As the geometry of the fluid and solid parts depends on the macroscopic coordinates, the microscopic parametric PDEs depend on the macroscopic coordinates around which the microscopic snapshot is taken. For a small number of parameters we solve the mapped micro problems in a reference micro mesh. These solutions are called the reduced basis and they span the solution space. For an arbitrary parameter we approximate the exact FE solutions of the micro problems by projecting them into the low-dimensional solution space. Since we use a parameter-dependent test space, we obtain a Petrov-Galerkin method. The efficiency of such strategy is achieved via standard offline-online splitting.

The *offline stage* is run only once while constructing the RB space and precomputing the necessary quantities for the online stage. This stage is detailed in section 5.

The *online stage* provides a cheap evaluation of $a^{\mathrm{RB}}(x)$, an approximation of the effective permeability, for any macroscopic coordinate $x \in \Omega$. The computation time of a single online RB evaluation is independent of the reference micro mesh. Consequently, the computation time of the online RB-DS-FE-HMM is comparable to a single-scale Darcy problem.

4.1. Parametrization of the geometry. Assume that the map $\varphi(x,\cdot)$ from section 2.2 is known for every $x \in \Omega$ and that it is piecewise affine. Let $R \in \mathbb{N}$ and $\{Y_{\mathrm{F}}^r\}_{r=1}^R$ be a disjoint partition of Y_{F} into subdomains such that the restriction $\varphi(x,y)|_{y\in Y_{\mathrm{F}}^r}$ is linear for every fixed $x \in \Omega$ and $r \in \{1,\dots,R\}$. Precisely, we assume that there are vector fields $C^r : \Omega \to \mathbb{R}^d$ and tensor fields $G^r : \Omega \to \mathbb{R}^{d\times d}$ such that $\varphi(x,y)|_{y\in Y_{\mathrm{F}}^r} = C^r(x) + G^r(x)y$ for every $x \in \Omega$ and $r \in \{1,\dots,R\}$. For an illustration see Figure 3.

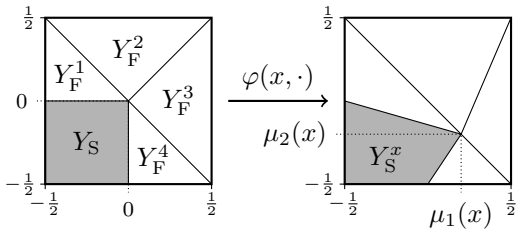

$$C^r(x) = \begin{pmatrix}\mu_1(x)\\ \mu_2(x)\end{pmatrix} \quad \text{for } r \in \{1,2,3,4\},$$

$$G^1(x) = \begin{pmatrix}1+2\mu_1(x) & 0\\ 2\mu_2(x) & 1\end{pmatrix}$$
$$G^2(x) = \begin{pmatrix}1 & -2\mu_1(x)\\ 0 & 1-2\mu_2(x)\end{pmatrix}$$
$$G^3(x) = \begin{pmatrix}1-2\mu_1(x) & 0\\ -2\mu_2(x) & 1\end{pmatrix}$$
$$G^4(x) = \begin{pmatrix}1 & 2\mu_1(x)\\ 0 & 1+2\mu_2(x)\end{pmatrix}$$

Figure 3: A reference micro geometry Y_{F} with $R = 4$ subdomains. The local pore geometries $(Y_{\mathrm{S}}^x, Y_{\mathrm{F}}^x)$ are defined by $\varphi(x,\cdot)$ that maps the corner of the L-shape of Y_{F} from $(0,0)$ to $\mu(x)$, where $\mu : \Omega \to Y$ is a given function.

Remark 2. In the description of the RB-DS-FE-HMM we consider Ω to be the parametric space and $x \in \Omega$ to be the parameter. The RB method is then used to approximate (5) in the family of micro geometries $\{(Y_{\mathrm{S}}^x, Y_{\mathrm{F}}^x)\}_{x\in\Omega}$. It is sometimes convenient (see Figure 3 and section 8) to define a family of micro geometries $\{(Y_{\mathrm{S}}^\mu, Y_{\mathrm{F}}^\mu)\}_{\mu\in\mathcal{D}}$, where $\mathcal{D} \subset \mathbb{R}^p$ is a parametric domain. To define a porous structure in Ω it is then sufficient to provide a mapping $\mu : \Omega \to \mathcal{D}$ and define local pore geometries as $(Y_{\mathrm{S}}^x, Y_{\mathrm{F}}^x) := (Y_{\mathrm{S}}^{\mu(x)}, Y_{\mathrm{F}}^{\mu(x)})$.

Micro problems in the reference domain. We now pull back the Stokes micro problem (8) from Y_{F}^x to Y_{F} using the change of variables $\varphi(x,\cdot)^{-1} : Y_{\mathrm{F}}^x \to Y_{\mathrm{F}}$. The resulting

problem reads as follows: Find $(\mathbf{u}^{i,x,\mathrm{e}}, p^{i,x,\mathrm{e}}, \lambda^{i,x,\mathrm{e}}) \in X = W(Y_\mathrm{F}) \times L^2(Y_\mathrm{F}) \times \mathbb{R}$ such that

$$\begin{aligned} a(\mathbf{u}^{i,x,\mathrm{e}}, \mathbf{v}; x) + b(\mathbf{v}, p^{i,x,\mathrm{e}}; x) + b(\mathbf{u}^{i,x,\mathrm{e}}, q; x) \\ + c(q, \lambda^{i,x,\mathrm{e}}; x) + c(p^{i,x,\mathrm{e}}, \kappa; x) = g^i(\mathbf{v}; x) \end{aligned} \tag{18}$$

for every $(\mathbf{v}, q, \kappa) \in X$. The superscript e stands for *exact solution*. The linear and bilinear forms in (18) depend on $x \in \Omega$. Indeed, we have

$$\begin{aligned} a(\mathbf{u}, \mathbf{v}; x) &= \sum_{r=1}^{R} \sum_{i,j=1}^{d} \nu_{ij}^{r,x} \int_{Y_\mathrm{F}^r} \frac{\partial \mathbf{u}}{\partial y_i} \cdot \frac{\partial \mathbf{v}}{\partial y_j} \,\mathrm{d}y, \quad c(q, \kappa; x) = \kappa \sum_{r=1}^{R} J^r(x) \int_{Y_\mathrm{F}^r} q \,\mathrm{d}y, \\ b(\mathbf{v}, q; x) &= -\sum_{r=1}^{R} \sum_{i,j=1}^{d} \kappa_{ij}^{r,x} \int_{Y_\mathrm{F}^r} q \frac{\partial \mathbf{v}_i}{\partial y_j} \,\mathrm{d}y, \qquad g^i(\mathbf{v}; x) = \sum_{r=1}^{R} J^r(x) \int_{Y_\mathrm{F}^r} \mathbf{v}_i \,\mathrm{d}y, \end{aligned} \tag{19}$$

where $J^r(x) = \det(G^r(x))$, $\nu^{r,x} = J^r(x) G^r(x)^{-1} G^r(x)^{-T}$, and $\kappa^{r,x} = J^r(x) G^r(x)^{-T}$. For any $\mathbf{U} = (\mathbf{u}, p, \lambda)$ and $\mathbf{V} = (\mathbf{v}, q, \kappa)$ we can now define $A(\mathbf{U}, \mathbf{V}; x)$ as the left-hand side of (18) and $G^i(\mathbf{V}; x) = g^i(\mathbf{v}; x)$, which allows us to abbreviate (18) as: Find $\mathbf{U}_\mathrm{e}^{i,x} = (\mathbf{u}^{i,x,\mathrm{e}}, p^{i,x,\mathrm{e}}, \lambda^{i,x,\mathrm{e}}) \in X$ such that

$$A(\mathbf{U}_\mathrm{e}^{i,x}, \mathbf{V}; x) = G^i(\mathbf{V}; x) \qquad \forall \mathbf{V} \in X. \tag{20}$$

The solutions to (20) are equivalent to those of (8) or (5) up to the change of variables, that is, $\mathbf{u}^{i,x}(\varphi(x, y)) \equiv \mathbf{u}^{i,x,\mathrm{e}}(y)$. Hence, the effective permeability (6) reads

$$a_{ij}^0(x) = g^i(\mathbf{u}^{j,x}) = g^i(\mathbf{u}^{j,x,\mathrm{e}}; x) = G^i(\mathbf{U}_\mathrm{e}^{j,x}; x) \qquad \forall i, j \in \{1, \dots, d\}. \tag{21}$$

Well-posedness of (20)**.** The micro problems (5), (8) and (20) are equivalent but their stability constants are defined differently. Instead of the Brezzi inf-sup condition (7) (saddle-point problem), one requires for (20) the Babuška inf-sup condition (non-coercive problem)

$$\beta_\mathrm{Ba}(x) = \inf_{\mathbf{U} \in X} \sup_{\mathbf{V} \in X} \frac{A(\mathbf{U}, \mathbf{V}; x)}{\|\mathbf{U}\|_X \|\mathbf{V}\|_X} > 0. \tag{22}$$

Equivalence of these formulations and relation between the Brezzi and Babuška constants have been studied in [23, 37, 45]. Non-degeneracy of the mapping $\varphi(x, y)$ also ensures continuity of $A(\cdot, \cdot; x)$ and $F(\cdot; x)$, that is, there are $\gamma_A(x), \gamma_G^i(x) \in \mathbb{R}$ such that

$$\begin{aligned} A(\mathbf{U}, \mathbf{V}; x) &\le \gamma_A(x) \|\mathbf{U}\|_X \|\mathbf{V}\|_X \qquad && \forall \mathbf{U}, \mathbf{V} \in X, \\ G^i(\mathbf{V}; x) &\le \gamma_G^i(x) \|\mathbf{V}\|_X && \forall \mathbf{V} \in X. \end{aligned} \tag{23}$$

Affine decomposition. Using the relations (19) we easily obtain an affine decomposition of the micro problem (20). Consider

- symmetric bilinear forms $A^q(\cdot, \cdot) : X \times X \to \mathbb{R}$ for $q \in \{1, \dots, Q_A\}$, where $Q_A \in \mathbb{N}$,
- linear forms $G^{iq}(\cdot) : X \to \mathbb{R}$ for $q \in \{1, \dots, Q_G\}$ and $i \in \{1, \dots, d\}$, where $Q_G \in \mathbb{N}$,
- vector fields $\Theta^A : \Omega \to \mathbb{R}^{Q_A}$ and $\Theta^G : \Omega \to \mathbb{R}^{Q_G}$,

such that for any $\mathbf{U}, \mathbf{V} \in X$, parameter $x \in \Omega$, and $i \in \{1, \dots, d\}$ we have

$$A(\mathbf{U}, \mathbf{V}; x) = \sum_{q=1}^{Q_A} \Theta_q^A(x) A^q(\mathbf{U}, \mathbf{V}), \qquad G^i(\mathbf{V}; x) = \sum_{q=1}^{Q_G} \Theta_q^G(x) G^{iq}(\mathbf{V}). \tag{24}$$

Since the numbers Q_A and Q_G influence the time and memory requirements of the algorithm, one tries to minimize them. A direct application of (24) yields $Q_A \approx 2Rd^2$ and $Q_G \approx R$. It is often possible to reduce this complexity by symbolic manipulation of (24). In the example from Figure 3 we can obtain $Q_A = 15$ and $Q_G = 3$ with $\Theta^G(x) = (1, \mu_1, \mu_2)$. Another approach to reduce Q_A or Q_G is using the empirical interpolation method [13].

Discretization of (20)**.** Let $\mathcal{T}_\mathcal{N}$ be a conformal, shape-regular triangulation of Y_F, where $\mathcal{N}$ stands for the number of degrees of freedom in the equation (25) below. We further assume that $\mathcal{T}_\mathcal{N}$ is a submesh of $\{Y_\mathrm{F}^r\}_{r=1}^R$, that is, for every $K \in \mathcal{T}_\mathcal{N}$ there is $r \in \{1, \dots, R\}$ such that $K \subset Y_\mathrm{F}^r$. Consider the Taylor-Hood $\mathcal{P}^{k+1}/\mathcal{P}^k$ FE spaces (similar to (10)) given by

$$\begin{aligned} L_\mathcal{N} &= \{q \in S_\mathcal{N}^k(Y_\mathrm{F}); \qquad q \text{ is } Y\text{-periodic}\}, \\ W_\mathcal{N} &= \{\mathbf{v} \in S_\mathcal{N}^{k+1}(Y_\mathrm{F})^d; \quad \mathbf{v} \text{ is } Y\text{-periodic}, \quad \mathbf{v} = 0 \text{ on } \partial Y_\mathrm{S}\}. \end{aligned}$$

A discrete equivalent of X is now $X_{\mathcal{N}} = W_{\mathcal{N}} \times L_{\mathcal{N}} \times \mathbb{R}$. We define a numerical approximation of the problem (20) and the output of interest $a^0(x) \approx a^{\mathcal{N}}(x)$ as follows. Find $\mathbf{U}_{\mathcal{N}}^{i,x} = (\mathbf{u}^{i,x,\mathcal{N}}, p^{i,x,\mathcal{N}}, \lambda^{i,x,\mathcal{N}}) \in X_{\mathcal{N}}$ and such that

$$A(\mathbf{U}_{\mathcal{N}}^{i,x}, \mathbf{V}; x) = G^i(\mathbf{V}; x) \qquad \forall \mathbf{V} \in X_{\mathcal{N}}, \tag{25}$$

$$a_{ij}^{\mathcal{N}}(x) = G^i(\mathbf{U}_{\mathcal{N}}^{j,x}; x) \qquad \forall i, j \in \{1, \dots, d\}. \tag{26}$$

Scalar product on X. Stability of the RB method is measured with respect to a norm on X that corresponds to a scalar product. It is advised (see [37,38]) that this induced norm is uniformly equivalent to the H^1-norm with respect to $\mathcal{N}$. A standard choice is

$$(\mathbf{U}, \mathbf{V})_X = (\nabla \mathbf{u}, \nabla \mathbf{v})_{L^2(Y_{\mathrm{F}})} + \tau(\mathbf{u}, \mathbf{v})_{L^2(Y_{\mathrm{F}})} + (p, q)_{L^2(Y_{\mathrm{F}})} + \lambda\kappa, \tag{27}$$

where $\mathbf{U} = (\mathbf{u}, p, \lambda)$ and $\mathbf{V} = (\mathbf{v}, q, \kappa)$ and $\tau > 0$ is a numerical approximation to the optimal constant from the Poincaré–Friedrichs inequality: $|\mathbf{w}^{\mathcal{N}}|_{H^1(Y_{\mathrm{F}})} \geq \tau \|\mathbf{w}^{\mathcal{N}}\|_{L^2(Y_{\mathrm{F}})}$ for every $\mathbf{w}^{\mathcal{N}} \in W_{\mathcal{N}}$. Accurate values of τ improve the efficiency of the eigensolvers needed in section 5.3 (see [26,37]).

Well-posedness of (25). The continuity constants of $A(\cdot, \cdot; x) : X_{\mathcal{N}} \times X_{\mathcal{N}} \to \mathbb{R}$ and $F(\cdot; x) : X_{\mathcal{N}} \to \mathbb{R}$ are bounded above by the constants in (23). Using stable FE spaces ensures that

$$\beta_{\mathrm{Ba}}^{\mathcal{N}}(x) = \inf_{\mathbf{U} \in X_{\mathcal{N}}} \sup_{\mathbf{V} \in X_{\mathcal{N}}} \frac{A(\mathbf{U}, \mathbf{V}; x)}{\|\mathbf{U}\|_X \|\mathbf{V}\|_X} > 0. \tag{28}$$

4.2. Reduced basis formulation. We consider (25) as d independent problems indexed by $i \in \{1, \dots, d\}$. We project (25) to a solution space $X_i \subset X_{\mathcal{N}}$ and a parameter-dependent test space $Y_i^x \subset X_{\mathcal{N}}$, both of dimension $N_i \ll \mathcal{N}$. The solution space X_i is spanned by a small number of solutions of (25) computed for parameter values $S^i = \{x^{i,1}, x^{i,2}, \dots, x^{i,N_i}\} \subset \Omega$. For every $n = 1, 2, \dots, N_i$ we denote by $\mathbf{U}_{\mathcal{N}}^{i,n} \in X_{\mathcal{N}}$ the solution to (25) with $x = x^{i,n} \in S^i$. The sequence $\{\mathbf{U}_{\mathcal{N}}^{i,n}\}_n$ is then orthonormalized by the Gram–Schmidt method (without changing the notation) to achieve algebraic stability (section 5.5). We then define $X_i = \operatorname{span}\{\mathbf{U}_{\mathcal{N}}^{i,1}, \dots, \mathbf{U}_{\mathcal{N}}^{i,N_i}\}$. The RB approximation of (25) is then defined as follows: For any $x \in \Omega$ and $i \in \{1, \dots, d\}$ we search $\mathbf{U}_{\mathrm{RB}}^{i,x} \in X_i$ such that

$$A(\mathbf{U}_{\mathrm{RB}}^{i,x}, \mathbf{V}; x) = G^i(\mathbf{V}; x) \qquad \forall \mathbf{V} \in Y_i^x. \tag{29}$$

The inf-sup stability of the reduced problem (29) is guaranteed by an adequate construction of the test space Y_i^x. Consider the so-called *supremizer* operator $T : X_{\mathcal{N}} \times \Omega \to X_{\mathcal{N}}$. For any $x \in \Omega$ and $\mathbf{U} \in X_{\mathcal{N}}$ let $T(\mathbf{U}; x)$ be the Riesz's representant of $A(\mathbf{U}, \cdot; x)$, that is,

$$(T(\mathbf{U}; x), \mathbf{V})_X = A(\mathbf{U}, \mathbf{V}; x) \qquad \forall \mathbf{V} \in X_{\mathcal{N}}. \tag{30}$$

One can easily show that the supremizer operator $T(\cdot; x) : X_{\mathcal{N}} \to X_{\mathcal{N}}$ is linear and

$$T(\mathbf{U}; x) = \arg\max_{\mathbf{V} \in X_{\mathcal{N}}} \frac{A(\mathbf{U}, \mathbf{V}; x)}{\|\mathbf{V}\|_X}, \qquad \beta_{\mathrm{Ba}}^{\mathcal{N}}(x) = \inf_{\mathbf{U} \in X_{\mathcal{N}}} \frac{\|T(\mathbf{U}; x)\|_X}{\|\mathbf{U}\|_X}. \tag{31}$$

We now set

$$Y_i^x = T(X_i; x) = \operatorname{span}\{T(\mathbf{U}_{\mathcal{N}}^{i,1}; x), \dots, T(\mathbf{U}_{\mathcal{N}}^{i,N_i}; x)\}, \tag{32}$$

We describe a practical construction of the sets S^i in section 5.1.

Output of interest. A simple approximation of the output of interest (26) is $G^i(\mathbf{U}_{\mathrm{RB}}^{j,x}; x)$, which is optimal for $i = j$. However, if $i \neq j$, one can increase the order of accuracy with a dual RB problem [34]. Since the right-hand sides of our problems ($G^i(\cdot; x)$) are the same linear forms as needed to obtain the outputs of interest (26), we do not need to solve any additional dual problems. We thus define

$$a_{ij}^{\mathrm{RB}}(x) = G^i(\mathbf{U}_{\mathrm{RB}}^{j,x}; x) + R^j(\mathbf{U}_{\mathrm{RB}}^{i,x}; x), \tag{33}$$

where the residual $R^j : X \times \Omega \to \mathbb{R}$ is given by

$$\begin{aligned} R^j(\mathbf{V}; x) &= G^j(\mathbf{V}; x) - A(\mathbf{U}_{\mathrm{RB}}^{j,x}, \mathbf{V}; x) \\ &= A(\mathbf{U}_{\mathcal{N}}^{j,x} - \mathbf{U}_{\mathrm{RB}}^{j,x}, \mathbf{V}; x). \end{aligned} \tag{34}$$

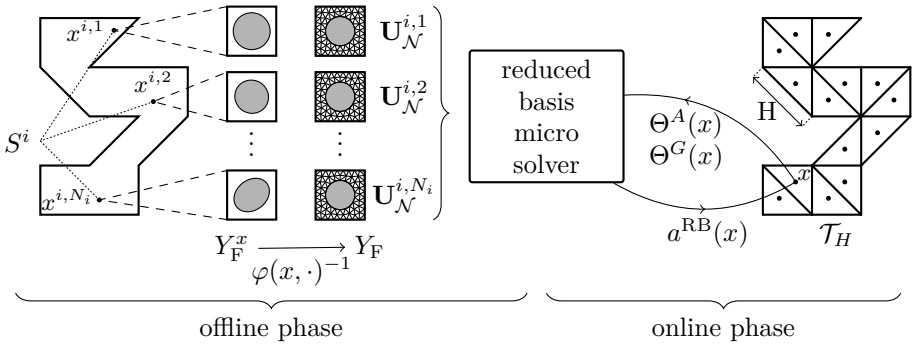

Figure 4: A sketch of the RB-DS-FE-HMM.

Well-posedness of (29)**.** The boundedness of $A(\cdot,\cdot;x)$ and $G^i(\cdot;x)$ over $X_{\mathcal{N}}$ is implied by (23). It has been shown that the inf-sup stability constant in the reduced equation (29) is preserved [4, 36], that is, for every $x \in \Omega$ and $i \in \{1,\dots,d\}$ we have

$$\beta_{\mathrm{Ba}}^i(x) := \inf_{\mathbf{U}\in X_i} \sup_{\mathbf{V}\in Y_i^x} \frac{A(\mathbf{U},\mathbf{V};x)}{\|\mathbf{U}\|_X \|\mathbf{V}\|_X} \geq \beta_{\mathrm{Ba}}^{\mathcal{N}}(x). \tag{35}$$

4.3. RB solution evaluation. Using the affine decomposition of $A(\cdot,\cdot;x)$ from (24) in the definition of $T(\cdot;x)$ from (30), we can deduce that $T(\mathbf{U};x) = \sum_{q=1}^{Q_A} \Theta_q^A(x) T^q(\mathbf{U})$, where $T^q(\mathbf{U})$ is the Riesz's representant of $A^q(\mathbf{U},\cdot)$, that is,

$$(T^q(\mathbf{U}),\mathbf{V})_X = A^q(\mathbf{U},\mathbf{V}) \qquad \forall \mathbf{V} \in X_{\mathcal{N}}. \tag{36}$$

This affine decomposition of $T(\cdot;x)$ allows us to write the basis functions of Y_i^x from (32) as linear combinations: $T(\mathbf{U}_{\mathcal{N}}^{i,n};x) = \sum_{q=1}^{Q_A} \Theta_q^A(x) T^q(\mathbf{U}_{\mathcal{N}}^{i,n})$. Hence, functions $\mathbf{U}_{\mathrm{RB}}^{i,x} \in X_i$ and $\mathbf{V} \in Y_i^x$ from (29) can be written as linear combinations

$$\mathbf{U}_{\mathrm{RB}}^{i,x} = \sum_{n=1}^{N_i} \overline{U}_n^{i,x} \mathbf{U}_{\mathcal{N}}^{i,n}, \qquad \mathbf{V} = \sum_{m=1}^{N_i} \overline{V}_m \sum_{q=1}^{Q_A} \Theta_q^A(x) T^q(\mathbf{U}_{\mathcal{N}}^{i,m}), \tag{37}$$

where $(\overline{U}_1^{i,x},\dots,\overline{U}_{N_i}^{i,x})^T, (\overline{V}_1,\dots,\overline{V}_{N_i})^T \in \mathbb{R}^{N_i}$ are vectors of coefficients. Plugging (37) into the reduced system (29), using the affine decomposition (24), and expanding and regrouping terms gives the following problem: find $\overline{U}^{i,x} \in \mathbb{R}^{N_i}$ such that

$$\overline{\mathbf{A}}^{i,x} \overline{U}^{i,x} = \overline{\mathbf{G}}^{i,x}, \tag{38}$$

where the matrix $\overline{\mathbf{A}}^{i,x} \in \mathbb{R}^{N_i \times N_i}$ and the right-hand side vector $\overline{\mathbf{G}}^{i,x} \in \mathbb{R}^{N_i}$ are given by

$$\overline{\mathbf{A}}^{i,x} = \sum_{q,r=1}^{Q_A} \Theta_q^A(x) \Theta_r^A(x) \overline{M}^{iqr}, \qquad \overline{\mathbf{G}}^{i,x} = \sum_{q=1}^{Q_G} \sum_{r=1}^{Q_A} \Theta_q^G(x) \Theta_r^A(x) \overline{N}^{iqr}. \tag{39}$$

Here, the matrices $\overline{M}^{iqr} \in \mathbb{R}^{N_i \times N_i}$ and vectors $\overline{N}^{iqr} \in \mathbb{R}^{N_i}$ are given by

$$\begin{aligned} \overline{M}_{nm}^{iqr} &= A^q(\mathbf{U}_{\mathcal{N}}^{i,n}, T^r(\mathbf{U}_{\mathcal{N}}^{i,m})) = (T^q(\mathbf{U}_{\mathcal{N}}^{i,n}), T^r(\mathbf{U}_{\mathcal{N}}^{i,m}))_X, \\ \overline{N}_m^{iqr} &= G^{iq}(T^r(\mathbf{U}_{\mathcal{N}}^{i,m})). \end{aligned} \tag{40}$$

The values (40) are precomputed in the offline stage and the dense linear system (38) with N_i variables is assembled (via (39)) and solved in the online stage.

4.4. RB output evaluation. Assume that we have computed $\overline{U}^{i,x}$ for $i \in \{1,\dots,d\}$. We rewrite (33) using the affine decompositions (24) and (37) to obtain

$$a_{ij}^{\mathrm{RB}}(x) = \sum_{q=1}^{Q_G} \Theta_q^G(x) (\overline{S}^{ijq} \cdot \overline{U}^{j,x} + \overline{S}^{jiq} \cdot \overline{U}^{i,x}) - \sum_{q=1}^{Q_A} \Theta_q^A(x) \overline{T}^{jiq} \overline{U}^{j,x} \cdot \overline{U}^{i,x}, \tag{41}$$

where the vectors $\overline{S}^{ijq} \in \mathbb{R}^{N_j}$ and the matrices $\overline{T}^{ijq} \in \mathbb{R}^{N_i \times N_j}$ can be precomputed in the offline stage as

$$\overline{S}_n^{ijq} = G^{iq}(\mathbf{U}_{\mathcal{N}}^{j,n}), \qquad \overline{T}_{nm}^{ijq} = A^q(\mathbf{U}_{\mathcal{N}}^{i,n}, \mathbf{U}_{\mathcal{N}}^{j,m}). \tag{42}$$

5 Offline RB stage

In section 5.1 we recall an offline greedy algorithm to construct the parameter sets S^i. This algorithm uses a cheap a posteriori estimator of the RB error (section 5.2) that relies on a rigorous estimate of the stability constant (28) (section 5.3). One can derive a posteriori estimators for the output of interest (section 5.4) and a priori error analysis (section 5.5). We conclude by an analysis of computational cost in section 5.6.

5.1. Greedy construction of the RB. For every $i \in \{1, \dots, d\}$ we perform the selection of the RB parameters S^i once. We chose a standard greedy approach that adds points $x \in \Omega$ from a training set to S^i, until a suitable error tolerance is reached. The error $\|\mathbf{U}_{\mathcal{N}}^{i,x} - \mathbf{U}_{\mathrm{RB}}^{i,x}\|_X$ is estimated by its upper bound (see Lemma 4)

$$\Delta_i^{\mathrm{E}}(x) = \frac{\|R^i(\cdot; x)\|_{(X_{\mathcal{N}})'}}{\beta_{\mathrm{SCM}}(x)}, \tag{43}$$

where the residual R^i is defined in (34) and $\beta_{\mathrm{SCM}}(x)$ is a cheap computable positive lower bound of $\beta_{\mathrm{Ba}}^{\mathcal{N}}(x)$ that will be described in section 5.3.

Algorithm 3 (offline greedy RB construction)**.** Given $i \in \{1, \dots, d\}$, training set size $N_{\mathrm{train}}^{\mathrm{RB}} \in \mathbb{N}$, and tolerance $\varepsilon_{\mathrm{RB}} > 0$ do:

1. *Initialization.* Choose randomly (Monte Carlo) or structurally (regular grid) a training set $\Xi_{\mathrm{train}}^{\mathrm{RB}} \subset \Omega$ of size $N_{\mathrm{train}}^{\mathrm{RB}}$. Set $S^i = \emptyset$ and $N_i = 0$.
2. *Estimate.* For every $x \in \Xi_{\mathrm{train}}^{\mathrm{RB}}$ compute the RB error estimator (43) and let $\tilde{x} \in \Xi_{\mathrm{train}}^{\mathrm{RB}}$ be the argument for which $\Delta_i^{\mathrm{E}}(\tilde{x})$ is maximized.
3. *Stopping criterion.* If $\Delta_i^{\mathrm{E}}(\tilde{x}) < \varepsilon_{\mathrm{RB}}$, then we precompute (42) and stop the algorithm. Else, we let $N_i \leftarrow N_i + 1$, set $x^{i,N_i} = \tilde{x}$, and update $S^i \leftarrow S^i \cup \{x^{i,N_i}\}$.
4. *Update online fields.* Compute $\mathbf{U}_{\mathcal{N}}^{i,N_i}$ by solving (25) with $x = x^{i,N_i}$ and compute the supremizers $T^q(\mathbf{U}_{\mathcal{N}}^{i,N_i})$ for $q = 1, \dots, Q_A$ by solving (36). Update (40) and go to step 2.

When Algorithm 3 stops it gives S^i such that the RB error is bounded by $\varepsilon_{\mathrm{RB}}$ in all training points. We cannot guarantee this bound for all $x \in \Omega$ but one expects comparable errors if the training set is dense enough.

5.2. A posteriori error indicator. We prove that the error indicator $\Delta_i^{\mathrm{E}}(x)$ defined in (43) majorizes the RB error and we describe a cheap evaluation of $\Delta_i^{\mathrm{E}}(x)$.

Lemma 4. *For any $x \in \Omega$ and $i \in \{1, \dots, d\}$ we have $\|\mathbf{U}_{\mathcal{N}}^{i,x} - \mathbf{U}_{\mathrm{RB}}^{i,x}\|_X \le \Delta_i^{\mathrm{E}}(x)$.*

Proof. Using the inf-sup condition (28), definition (34), and inequality (48), gives

$$\|\mathbf{U}_{\mathcal{N}}^{i,x} - \mathbf{U}_{\mathrm{RB}}^{i,x}\|_X \le \frac{1}{\beta_{\mathrm{Ba}}^{\mathcal{N}}(x)} \sup_{\mathbf{V} \in X_{\mathcal{N}}} \frac{A(\mathbf{U}_{\mathcal{N}}^{i,x} - \mathbf{U}_{\mathrm{RB}}^{i,x}, \mathbf{V}; x)}{\|\mathbf{V}\|_X} \le \Delta_i^{\mathrm{E}}(x).$$

The inequality (48) establishes that $\beta_{\mathrm{SCM}}^{\mathcal{N}}(x) \le \beta_{\mathrm{Ba}}^{\mathcal{N}}(x)$, which concludes the proof. □

Evaluation of $\Delta_i^{\mathrm{E}}(x)$. From the error bound (43) we consider here only the evaluation of $\|R^i(\cdot; x)\|_{(X_{\mathcal{N}})'}$, following [38]. Evaluation of $\beta_{\mathrm{SCM}}(x)$ is presented in section 5.3. The residual $R^i(\cdot; x)$ is a linear functional on the Hilbert space $X_{\mathcal{N}}$, hence the Riesz representation theorem applies: there is a unique $\mathbf{E}_{\mathcal{N}}^{i,x} \in X_{\mathcal{N}}$ such that $(\mathbf{E}_{\mathcal{N}}^{i,x}, \mathbf{V})_X = R^i(\mathbf{V}; x)$ for every $\mathbf{V} \in X_{\mathcal{N}}$. We next find an affine decomposition of $\mathbf{E}_{\mathcal{N}}^{i,x}$. Recalling that (see (34) and (24))

$$\begin{aligned} R^i(\mathbf{V}; x) &= G^i(\mathbf{V}; x) - A(\mathbf{U}_{\mathrm{RB}}^{i,x}, \mathbf{V}; x) \\ &= \sum_{q=1}^{Q_G} \Theta_q^G(x) G^{iq}(\mathbf{V}) - \sum_{q=1}^{Q_A} \sum_{n=1}^{N_i} \Theta_q^A(x) \overline{U}_n^{i,x} A^q(\mathbf{U}_{\mathrm{RB}}^{i,x}, \mathbf{V}; x) \end{aligned}$$

and using the identity (36) we obtain

$$\mathbf{E}_{\mathcal{N}}^{i,x} = \sum_{q=1}^{Q_G} \Theta_q^G(x) \mathbf{G}_{\mathcal{N}}^{iq} - \sum_{q=1}^{Q_A} \sum_{n=1}^{N_i} \Theta_q^A(x) \overline{U}_n^{i,x} T^q(\mathbf{U}_{\mathcal{N}}^{i,n}), \tag{44}$$

where the Riesz's representant $\mathbf{G}^{iq}_{\mathcal{N}} \in X_{\mathcal{N}}$ satisfies $(\mathbf{G}^{iq}_{\mathcal{N}}, \mathbf{V})_X = G^{iq}(\mathbf{V})$ for every $\mathbf{V} \in X_{\mathcal{N}}$. Expanding the equality $\|R^i(\cdot;x)\|^2_{(X_{\mathcal{N}})'} = (\mathbf{E}^{i,x}_{\mathcal{N}}, \mathbf{E}^{i,x}_{\mathcal{N}})_X$ using (44) yields

$$\begin{aligned}\|R^i(\cdot;x)\|^2_{(X_{\mathcal{N}})'} &= \sum_{q,r=1}^{Q_G} \Theta^G_q(x)\Theta^G_r(x)\overline{P}^{iqr} - 2\sum_{q=1}^{Q_G}\sum_{r=1}^{Q_A} \Theta^G_q(x)\Theta^A_r(x)\overline{N}^{iqr}\cdot\overline{U}^{i,x} \\ &\quad + \sum_{q,r=1}^{Q_A} \Theta^A_q(x)\Theta^A_r(x)\overline{M}^{iqr}\overline{U}^{i,x}\cdot\overline{U}^{i,x} \\ &= \sum_{q,r=1}^{Q_G} \Theta^G_q(x)\Theta^G_r(x)\overline{P}^{iqr} - 2\overline{\mathbf{G}}^{i,x}\cdot\overline{U}^{i,x} + \overline{\mathbf{A}}^{i,x}\overline{U}^{i,x}\cdot\overline{U}^{i,x},\end{aligned} \tag{45}$$

where we used the definition (40) for $\overline{N}^{iqr}$ and $\overline{M}^{iqr}$ and the numbers $\overline{P}^{iqr} \in \mathbb{R}$ can be precomputed in the offline stage by $\overline{P}^{iqr} = (\mathbf{G}^{iq}_{\mathcal{N}}, \mathbf{G}^{ir}_{\mathcal{N}})_X$.

5.3. Successive constraint method (SCM). Here we describe a cheap lower bound $\beta_{\mathrm{SCM}}(x)$ of the inf-sup constant $\beta^{\mathcal{N}}_{\mathrm{Ba}}(x)$. We follow the algorithm [26] with some modifications detailed in Remark 7. Using (28) and (31) for any $x, \overline{x} \in \Omega$ we have

$$\begin{aligned}\beta^{\mathcal{N}}_{\mathrm{Ba}}(x) &\geq \inf_{\mathbf{U}\in X_{\mathcal{N}}} \frac{A(\mathbf{U}, T(\mathbf{U};\overline{x});x)}{\|\mathbf{U}\|_X \|T(\mathbf{U};\overline{x})\|_X} \\ &\geq \underbrace{\inf_{\mathbf{U}\in X_{\mathcal{N}}} \frac{\|T(\mathbf{U};\overline{x})\|_X}{\|\mathbf{U}\|_X}}_{=\beta^{\mathcal{N}}_{\mathrm{Ba}}(\overline{x})} \underbrace{\inf_{\mathbf{U}\in X_{\mathcal{N}}} \frac{A(\mathbf{U}, T(\mathbf{U};\overline{x});x)}{\|T(\mathbf{U};\overline{x})\|^2_X}}_{=:\overline{\beta}^{\mathcal{N}}(x;\overline{x})}.\end{aligned} \tag{46}$$

The SCM uses a greedy algorithm to construct a finite set $S \subset \Omega$ and a family of finite sets $\{C_{\overline{x}}\}_{\overline{x}\in S} \subset \Omega$ such that:

- for each $\overline{x} \in S$ the value $\beta^{\mathcal{N}}_{\mathrm{Ba}}(\overline{x})$ is computed and stored,
- given a $\overline{x} \in S$ the values $\overline{\beta}^{\mathcal{N}}(x;\overline{x})$ are computed and stored for every $x \in C_{\overline{x}}$. They are used to provide cheap bounds of $\overline{\beta}^{\mathcal{N}}(x;\overline{x})$ defined in (52) that satisfy

$$\beta^{\mathrm{LB}}(x;\overline{x},C) \leq \overline{\beta}^{\mathcal{N}}(x;\overline{x}) \leq \beta^{\mathrm{UB}}(x;\overline{x},C) \qquad \forall x \in \Omega \tag{47}$$

  for any nonempty set $C \subset \Omega$.

Using (46) and (47) we obtain (and define)

$$\beta^{\mathcal{N}}_{\mathrm{Ba}}(x) \geq \beta_{\mathrm{SCM}}(x) := \max_{\overline{x}\in S} \beta^{\mathcal{N}}_{\mathrm{Ba}}(\overline{x})\beta^{\mathrm{LB}}(x;\overline{x},C_{\overline{x}}). \tag{48}$$

In the next subsections we explain the construction of the bounds (47).

5.3.1. Eigenproblems. The values of $\beta^{\mathcal{N}}_{\mathrm{Ba}}(\overline{x})$ or $\overline{\beta}^{\mathcal{N}}(x;\overline{x})$ described in (46) can be interpreted as minimal eigenvalues of a related eigenproblem. If we denote

$$\mathbf{U}^{x,\overline{x}}_{\mathcal{N}} = \arg\min_{\mathbf{U}\in X_{\mathcal{N}}} \begin{cases} \dfrac{A(\mathbf{U}, T(\mathbf{U};\overline{x});x)}{\|T(\mathbf{U};\overline{x})\|^2_X} & \text{if } \overline{x} \neq x, \\ \dfrac{\|T(\mathbf{U};\overline{x})\|_X}{\|\mathbf{U}\|_X} & \text{if } \overline{x} = x, \end{cases} \tag{49}$$

we can then express

$$\begin{aligned}\beta^{\mathcal{N}}_{\mathrm{Ba}}(\overline{x}) &= \frac{\|T(\mathbf{U}^{\overline{x},\overline{x}}_{\mathcal{N}};\overline{x})\|_X}{\|\mathbf{U}^{\overline{x},\overline{x}}_{\mathcal{N}}\|_X}, \\ \overline{\beta}^{\mathcal{N}}(x;\overline{x}) &= \frac{A(\mathbf{U}^{x,\overline{x}}_{\mathcal{N}}, T(\mathbf{U}^{x,\overline{x}}_{\mathcal{N}};\overline{x});x)}{\|T(\mathbf{U}^{x,\overline{x}}_{\mathcal{N}};\overline{x})\|^2_X} = \sum_{q=1}^{Q_A} \Theta^A_q(x) \underbrace{\frac{A^q(\mathbf{U}^{x,\overline{x}}_{\mathcal{N}}, T(\mathbf{U}^{x,\overline{x}}_{\mathcal{N}};\overline{x}))}{\|T(\mathbf{U}^{x,\overline{x}}_{\mathcal{N}};\overline{x})\|^2_X}}_{=:z_q(x;\overline{x})}.\end{aligned} \tag{50}$$

5.3.2. Upper and lower bounds. Let us fix a parameter $\overline{x} \in \Omega$. Using the affine decomposition (24) we obtain

$$\overline{\beta}^{\mathcal{N}}(x;\overline{x}) = \inf_{\mathbf{U}\in X_{\mathcal{N}}} \sum_{q=1}^{Q_A} \Theta_q^A(x) \frac{A^q(\mathbf{U}, T(\mathbf{U};\overline{x}))}{\|T(\mathbf{U};\overline{x})\|_X^2} = \inf_{z\in\mathcal{Y}_{\overline{x}}} \sum_{q=1}^{Q_A} \Theta_q^A(x) z_q, \tag{51}$$

where $\mathcal{Y}_{\overline{x}}$ is the set of all $z \in \mathbb{R}^{Q_A}$ such that $z_q = A^q(\mathbf{U}, T(\mathbf{U};\overline{x}))/\|T(\mathbf{U};\overline{x})\|_X^2$ for every $q \in \{1,\dots,Q_A\}$ for some $\mathbf{U} \in X_{\mathcal{N}}$. Given an arbitrary nonempty set $C \subset \Omega$, we can construct a chain of sets $\mathcal{Y}_{\overline{x}}^{\mathrm{UB}}(C) \subset \mathcal{Y}_{\overline{x}} \subset \mathcal{Y}_{\overline{x}}^{\mathrm{LB}}(C)$ (for a proof see [26]) by

$$\begin{aligned}
\mathcal{Y}_{\overline{x}}^{\mathrm{UB}}(C) &= \{z(\hat{x};\overline{x}) = (z_q(\hat{x};\overline{x}))_{q=1}^{Q_A} \in \mathbb{R}^{Q_A} : \hat{x} \in C\},\\
\mathcal{Y}_{\overline{x}}^{\mathrm{LB}}(C) &= \{(s_1,\dots,s_{Q_A}) \in \mathbb{R}^{Q_A} : |s_q| \le \gamma_q/\beta_{\mathrm{Ba}}^{\mathcal{N}}(\overline{x}) \quad \forall q \in \{1,\dots,Q_A\}\\
&\qquad \text{and } \textstyle\sum_{q=1}^{Q_A} \Theta_q^A(\hat{x}) s_q \ge \beta^{\mathcal{N}}(\hat{x};\overline{x}) \quad \forall \hat{x} \in C\},
\end{aligned}$$

where $\gamma_q = \sup_{\mathbf{U}\in X_{\mathcal{N}}} \|T^q(\mathbf{U})\|_X/\|\mathbf{U}\|_X$. We then define

$$\beta^{\mathrm{LB}}(x;\overline{x},C) = \min_{z\in\mathcal{Y}_{\overline{x}}^{\mathrm{LB}}(C)} \sum_{q=1}^{Q_A} \Theta_q^A(x) z_q, \qquad \beta^{\mathrm{UB}}(x;\overline{x},C) = \min_{z\in\mathcal{Y}_{\overline{x}}^{\mathrm{UB}}(C)} \sum_{q=1}^{Q_A} \Theta_q^A(x) z_q. \tag{52}$$

Using (51) and the inclusion property $\mathcal{Y}_{\overline{x}}^{\mathrm{UB}}(C) \subset \mathcal{Y}_{\overline{x}} \subset \mathcal{Y}_{\overline{x}}^{\mathrm{LB}}(C)$ we immediately get (47).

5.3.3. Greedy SCM algorithm. We next present an algorithm for constructing the set $S \subset \Omega$ and the family $\{C_{\overline{x}}\}_{\overline{x}\in S}$.

Algorithm 5 (offline greedy SCM construction)**.** Given a training size $N_{\mathrm{train}}^{\mathrm{SCM}} \in \mathbb{N}$, a tolerance $\varepsilon_{\mathrm{SCM}} \in (0,1)$, and $\theta \in (0,1)$ do:

1. *Initialization.* Choose randomly (Monte Carlo) or structurally (regular grid) a training set $\Xi_{\mathrm{train}}^{\mathrm{SCM}} \subset \Omega$ of size $N_{\mathrm{train}}^{\mathrm{SCM}}$. Compute γ_q for $q \in \{1,\dots,Q_A\}$. Let $S = \emptyset$ and $C_{\overline{x}} = \emptyset$ for every $\overline{x} \in \Omega$. Select a random $\overline{x} \in \Xi_{\mathrm{train}}^{\mathrm{SCM}}$ and set $\hat{x} \leftarrow \overline{x}$.
2. *Update.* Set $S \leftarrow S \cup \{\overline{x}\}$ and $C_{\overline{x}} \leftarrow C_{\overline{x}} \cup \{\hat{x}\}$. Compute $\mathbf{U}_{\mathcal{N}}^{\hat{x},\overline{x}}$ by solving the eigenproblem (49) and use it to obtain $z_q(\hat{x};\overline{x})$ defined in (50).
3. *Upper bound check.* Find the training point $\hat{x} \in \Xi_{\mathrm{train}}^{\mathrm{SCM}}$ with the smallest upper bound estimate by
$$\hat{x} \leftarrow \arg\min_{\hat{x}\in\Xi_{\mathrm{train}}^{\mathrm{SCM}}} \max_{\overline{x}\in S} \beta^{\mathrm{UB}}(\hat{x};\overline{x},C_{\overline{x}}).$$
If $\max_{\overline{x}\in S} \beta^{\mathrm{UB}}(\hat{x};\overline{x},C_{\overline{x}}) < \theta$, then we let $\overline{x} \leftarrow \hat{x}$ and continue with the step 2, which enlarges the set S with $\overline{x}$.
4. *Lower bound check.* Find a training point $\hat{x} \in \Xi_{\mathrm{train}}^{\mathrm{SCM}}$ and $\overline{x} \in S$ corresponding to the smallest lower bound estimate by
$$[\hat{x},\overline{x}] \leftarrow \arg\min_{\hat{x}\in\Xi_{\mathrm{train}}^{\mathrm{SCM}}} \max_{\overline{x}\in S} \{\beta_{\mathrm{LB}}(\hat{x};\overline{x},C_{\overline{x}});\ \beta_{\mathrm{UB}}(\hat{x};\overline{x},C_{\overline{x}}) \ge \theta\}.$$
If $\beta_{\mathrm{LB}}(\hat{x};\overline{x},C_{\overline{x}}) < \theta\varepsilon_{\mathrm{SCM}}$, then we continue with the step 2, which enlarges the set $C_{\overline{x}}$. Else, we have reached the tolerance and we stop the algorithm.

When Algorithm 5 stops we have $\beta_{\mathrm{SCM}}(x) > 0$ for all training points. We cannot guarantee positivity for every $x \in \Omega$ but we practically observe it, if the training set is dense enough.

Remark 6 (online SCM)**.** For any $x \in \Omega$ we get $\beta_{\mathrm{SCM}}(x)$ defined in (48) by computing $\beta_{\mathrm{LB}}(x;\overline{x},C_{\overline{x}})$ by solving the linear programming problem (52) for each $\overline{x} \in S$.

Remark 7. In the original procedure (see [26]) for each $\overline{x} \in S$ a corresponding set $C_{\overline{x}}$ is constructed before adding another element to S. This approach resulted in unnecessary large sets $C_{\overline{x}}$, therefore, we decided to construct all these sets concurrently. Furthermore, the precision of the SCM in [26] was controlled by a function $\varphi(x,\overline{x})$ that can be constructed using the so-called SCM^2 method. Since we don't expect extreme variations of $\beta_{\mathrm{Ba}}^{\mathcal{N}}(x)$, we replaced this function by a constant $\theta > 0$. In practice we chose $\theta = \varepsilon_{\mathrm{SCM}} = 0.5$.

5.4. A posteriori error estimate for $a^{\mathrm{RB}}(x)$. We discuss here the error between the permeability tensor $a^{\mathcal{N}}(x)$ and its RB approximation $a^{\mathrm{RB}}(x)$, defined in (26) and (33), respectively. Using the definitions (26) and (33), the residual definition (34), the problem statement (25), and symmetry of $A(\cdot,\cdot;x)$, we obtain the following identity

$$\begin{aligned} a^{\mathcal{N}}_{ij}(x) - a^{\mathrm{RB}}_{ij}(x) &= G^i(\mathbf{U}^{j,x}_{\mathcal{N}};x) - G^i(\mathbf{U}^{j,x}_{\mathrm{RB}};x) - G^j(\mathbf{U}^{i,x}_{\mathrm{RB}};x) + A(\mathbf{U}^{j,x}_{\mathrm{RB}},\mathbf{U}^{i,x}_{\mathrm{RB}};x) \\ &= A(\mathbf{U}^{i,x}_{\mathcal{N}} - \mathbf{U}^{i,x}_{\mathrm{RB}}, \mathbf{U}^{j,x}_{\mathcal{N}} - \mathbf{U}^{j,x}_{\mathrm{RB}};x) \\ &= R^i(\mathbf{U}^{j,x}_{\mathcal{N}} - \mathbf{U}^{j,x}_{\mathrm{RB}};x). \end{aligned} \tag{53}$$

Lemma 8. *For any $i,j \in \{1,\dots,d\}$ we have*

$$|a^{\mathcal{N}}_{ij}(x) - a^{\mathrm{RB}}_{ij}(x)| \le \frac{1}{\beta_{\mathrm{SCM}}(x)} \|R^i(\cdot;x)\|_{(X_{\mathcal{N}})'} \|R^j(\cdot;x)\|_{(X_{\mathcal{N}})'}, \tag{54}$$

$$\|a^{\mathcal{N}}(x) - a^{\mathrm{RB}}(x)\|_F \le \frac{1}{\beta_{\mathrm{SCM}}(x)} \sum_{i=1}^{d} \|R^i(\cdot;x)\|^2_{(X_{\mathcal{N}})'} =: \Delta^{\mathrm{F}}(x). \tag{55}$$

Proof. Using (53) and Lemma 4 gives

$$\begin{aligned} |a^{\mathcal{N}}_{ij}(x) - a^{\mathrm{RB}}_{ij}(x)| &= |R^i(\mathbf{U}^{j,x}_{\mathcal{N}} - \mathbf{U}^{j,x}_{\mathrm{RB}};x)| \le \|R^i(\cdot;x)\|_{(X_{\mathcal{N}})'} \|\mathbf{U}^{j,x}_{\mathcal{N}} - \mathbf{U}^{j,x}_{\mathrm{RB}}\|_X \\ &\le \|R^i(\cdot;x)\|_{(X_{\mathcal{N}})'} \Delta^{\mathrm{E}}_j(x) = \Delta^{\mathrm{out}}_{ij}(x). \end{aligned}$$

This shows (54) and (55) follows. □

The error bound (55) is quadratic with respect to the error bound for the RB solution (43). This improvement of accuracy is due to the use of dual problem in the definition (33).

5.5. A priori error analysis. Using the inf-sup stability (35) and $Y^i_x = T(X^i;\mu)$ one can obtain optimality of the RB method.

Lemma 9. *For every $i,j \in \{1,\dots,d\}$ and $x \in \Omega$ we have*

$$\|\mathbf{U}^{i,x}_{\mathcal{N}} - \mathbf{U}^{i,x}_{\mathrm{RB}}\|_X \le \left(1 + \frac{\gamma_A(x)}{\beta^{\mathcal{N}}_{\mathrm{Ba}}(x)}\right) \inf_{\mathbf{V}\in X_i} \|\mathbf{U}^{i,x}_{\mathcal{N}} - \mathbf{V}\|_X,$$

$$|a^{\mathcal{N}}_{ij}(x) - a^{\mathrm{RB}}_{ij}(x)| \le \gamma_A(x) \left(1 + \frac{\gamma_A(x)}{\beta^{\mathcal{N}}_{\mathrm{Ba}}(x)}\right)^2 \inf_{\mathbf{V}\in X_i} \|\mathbf{U}^{i,x}_{\mathcal{N}} - \mathbf{V}\|_X \inf_{\mathbf{W}\in X_j} \|\mathbf{U}^{j,x}_{\mathcal{N}} - \mathbf{W}\|_X.$$

Proof. The proof of the first inequality is given in [12]. Using (53) we obtain

$$\begin{aligned} |a^{\mathcal{N}}_{ij}(x) - a^{\mathrm{RB}}_{ij}(x)| &= |A(\mathbf{U}^{i,x}_{\mathcal{N}} - \mathbf{U}^{i,x}_{\mathrm{RB}}, \mathbf{U}^{j,x}_{\mathcal{N}} - \mathbf{U}^{j,x}_{\mathrm{RB}};x)| \\ &\le \gamma_A(x) \|\mathbf{U}^{i,x}_{\mathcal{N}} - \mathbf{U}^{i,x}_{\mathrm{RB}}\|_X \|\mathbf{U}^{j,x}_{\mathcal{N}} - \mathbf{U}^{j,x}_{\mathrm{RB}}\|_X. \end{aligned}$$

We conclude the proof of the second inequality by applying the first one. □

For the practical application of the RB method, it is of great importance that the reduced systems governed by the matrix $\overline{\mathbf{A}}^{i,x}$ are numerically stable. It can be shown (see [4] for details) that the condition number of $\overline{\mathbf{A}}^{i,x}$ is bounded by $\gamma^2_A(x)(\beta^i_{\mathrm{Ba}}(x))^{-2}$.

Let us discuss a priori convergence rates of the RB greedy algorithm with respect to the number of RB functions N_i. We apply the general framework for greedy approximations of compact sets in Hilbert spaces [15]. For each $i \in \{1,\dots,d\}$, the RB methods approximates the solution manifold $\mathcal{M}^i = \{\mathbf{U}^{i,x}_{\mathcal{N}};\ x \in \Omega\} \subset X_{\mathcal{N}}$ with $X_i \subset X_{\mathcal{N}}$. Approximability of $\mathcal{M}^i$ by linear subspaces of $X_{\mathcal{N}}$ of dimension n is described by the Kolomogorov n-width

$$d_n(\mathcal{M}^i) = \inf_{\substack{Z\subset X_{\mathcal{N}} \\ \dim(Z)=n}} \sup_{\mathbf{U}\in\mathcal{M}^i} \operatorname{dist}(\mathbf{U},Z),$$

where $\operatorname{dist}(\mathbf{U},Z) = \min_{\mathbf{V}\in Z} \|\mathbf{U}-\mathbf{V}\|_X$. Algorithm 3 is, in terminology of [15], a weak greedy algorithm, provided that the a posteriori error estimator $\Delta^{\mathrm{E}}_i(x)$ is uniformly equivalent to the exact error $\operatorname{dist}(\mathbf{U}^{i,x}_{\mathrm{RB}}, X_i)$. Indeed, by (43), (23), and Lemma 9 we have

$$\begin{aligned} \Delta^{\mathrm{E}}_i(x) &= \sup_{\mathbf{V}\in X_{\mathcal{N}}} \frac{A(\mathbf{U}^{i,x}_{\mathcal{N}} - \mathbf{U}^{i,x}_{\mathrm{RB}}, \mathbf{V};x)}{\beta_{\mathrm{SCM}}(x)\|\mathbf{V}\|_X} \le \frac{\gamma_A(x)}{\beta_{\mathrm{SCM}}(x)} \|\mathbf{U}^{i,x}_{\mathcal{N}} - \mathbf{U}^{i,x}_{\mathrm{RB}}\|_X \\ &\le \frac{\gamma_A(x)}{\beta_{\mathrm{SCM}}(x)} \left(1 + \frac{\gamma_A(x)}{\beta^i_{\mathrm{Ba}}(x)}\right) \operatorname{dist}(\mathbf{U}^{i,x}_{\mathrm{RB}}, X_i), \end{aligned} \tag{56}$$

and from Lemma 4 we simply obtain $\operatorname{dist}(\mathbf{U}^{i,x}_{\mathrm{RB}}, X_i) \leq \Delta^{\mathrm{E}}_i(x)$. The analysis in [15] then shows that there is a constant $\gamma \in (0,1]$, depending only on the constants from (56), such that the following properties are true:

- If there are constants $M, \alpha > 0$ such that $d_n(\mathcal{M}^i) \leq Mn^{-\alpha}$ for all $n > 0$, then $\operatorname{dist}(\mathbf{U}^{i,x}_{\mathrm{RB}}, X_i) \leq CMN_i^{-\alpha}$, where C depends only on α and γ.
- If there are constants $M, a, \alpha > 0$ such that $d_n(\mathcal{M}^i) \leq Me^{-an^{\alpha}}$ for all $n \geq 0$, then $\operatorname{dist}(\mathbf{U}^{i,x}_{\mathrm{RB}}, X_i) \leq CMe^{-cN_i^{\beta}}$, where $\beta = \alpha/(\alpha+1)$ and the constants $C, c > 0$ depend only on α and γ.

5.6. Computational cost. Here we describe the computational cost of offline and online RB procedures. For a comparison to other methods see [4,24]. Let $N = \max\{N_1, \ldots, N_d\}$, where N_i is the dimension of the RB space X_i and let $Q = \max\{Q_A, Q_G\}$.

Online stage. Let $x \in \Omega$ be arbitrary. To obtain the RB coefficients $\overline{U}^{i,x}$ we need to assemble (39) and solve the dense system (38) with N_i variables, which can we do with $\mathcal{O}(Q^2N_i^2 + N_i^3)$ operations. Then, we evaluate $a^{\mathrm{RB}}(x)$ via (41) in additional $\mathcal{O}(QN^2)$.

To obtain $\Delta^{\mathrm{E}}_i(x)$ we evaluate (45) in $\mathcal{O}(Q^2 + N_i^2)$ operations and we compute $\beta_{\mathrm{SCM}}(x)$ as described in Remark 6. Computation of $\beta_{\mathrm{SCM}}(x)$ via (48) and (52) is dominated by solving a linear programming problem in $\mathbb{R}^{Q_A}$ with $2Q_A + |C_{\overline{x}}|$ constraints for each $\overline{x} \in S$.

Offline stage. The major sources of computational cost in the offline RB (Algorithm 3 and 5) stage can be split into four categories:

Solving sparse linear systems. In Algorithm 3 (step 4) we solve $\mathcal{O}(N)$ Stokes problems (25) and compute $\mathcal{O}(QN)$ supremizers ($T^q(\mathbf{U}^{i,n}_{\mathcal{N}})$ and $\mathbf{G}^{iq}_{\mathcal{N}}$), which can be done in $\mathcal{O}(N(N+Q)\mathcal{N})$, assuming a linear-time solver.

Assembling online fields. In Algorithm 3 (step 4) we assemble (40) and we also need (42) for the output of interest. This takes $\mathcal{O}(N^2Q^2\mathcal{N})$.

Residual calculation. In Algorithm 3 (step 2) we compute the error estimator $\Delta^{\mathrm{E}}_i(x)$ in each iteration of the algorithm at all training points, which costs $\mathcal{O}(N^3(Q^2+N)N^{\mathrm{RB}}_{\mathrm{train}})$. Furthermore, we compute (48) at $N^{\mathrm{RB}}_{\mathrm{train}}$ points.

SCM. In Algorithm 5 we compute several eigenproblems of size $\mathcal{N}$. First, Q_A eigenproblems are needed to obtain $\gamma \in \mathbb{R}^{Q_A}$. Second, we solve $|S| + J$ eigenproblems to obtain $\mathbf{U}^{x,\overline{x}}_{\mathcal{N}}$ given in (49), where $J := \sum_{\overline{x} \in S} |C_{\overline{x}}|$. Furthermore, in each iteration of Algorithm 5 we need to compute the upper and lower bounds (52) in the sampling points. Hence, in the whole offline SCM we need to solve $\mathcal{O}((J + |S|)N^{\mathrm{SCM}}_{\mathrm{train}})$ linear programming problems.

Memory requirements. The online RB stage (excluding the the computation of $\beta_{\mathrm{SCM}}(x)$) has $\mathcal{O}(Q^2N^2)$ memory complexity, which is independent of $\mathcal{N}$. Since one can discard the supremizers after the step 4 in every iteration of Algorithm 3, the memory requirements of the offline RB stage are only $\mathcal{O}((N+Q)\mathcal{N})$.

6 A priori and a posteriori error estimates

In this section we estimate the errors between the RB-DS-FE-HMM solution $p^{H,\mathrm{RB}}$ and the homogenized solution p^0. We follow the DS-FE-HMM error estimates (section 3.1), but we need to account for the additional error caused by the RB approximation.

Well-posedness of (16). The problem (16) is well-posed if $a^{\mathrm{RB}}(x)$ is uniformly elliptic and bounded over all macroscopic quadrature points $x \in \{Q^H\}$. Uniform ellipticity and boundedness of $a^{\mathcal{N}}(x)$ for a wide range of geometries can be shown using the general criteria developed in [2]. Uniform boundedness of $a^{\mathrm{RB}}(x)$ follows from the well-posedness of the RB approximation, see (23) and (35). By setting the tolerance $\varepsilon_{\mathrm{RB}} > 0$ small enough and using (55), we can ensure the coercivity of $a^{\mathrm{RB}}(x)$ at least for x in the RB training set $\Xi^{\mathrm{RB}}_{\mathrm{train}}$. If the training set is dense enough in Ω, we expect to have ellipticity of $a^{\mathrm{RB}}(x)$ for any $x \in \Omega$.

Preliminaries. To discuss the a priori error estimates, following [2,5,7], we introduce two additional problems to (2) and (16) that will help us to decompose the error $e = p^0 - p^{H,\mathrm{RB}}$ into three components, based on the main source of the error. Consider a DS-FE-HMM problem that solves (11) with the tensor $a^{\mathcal{N}}$ (instead of a^h) in (12). Solution to this problem is denoted by $p^H \in S^l_H(\Omega)/\mathbb{R}$. Further, let $p^{0,H} \in S^l_H(\Omega)/\mathbb{R}$ be a solution to (11) but with tensor a^0 (instead of a^h) in (12).

6.1. A priori error estimates. We decompose the error to three components: macro, micro, and RB error, which are denoted by e_{mac}, e_{mic}, and e_{RB}, respectively. Since we are working with the exact micro domains Y_{F}^x (compared to $Y_{\mathrm{F}}^{x,\delta}$ in DS-FE-HMM), the modeling error is not present. The triangle inequality gives

$$\underbrace{|p^0 - p^{H,\mathrm{RB}}|_{H^1(\Omega)}}_{e} \leq \underbrace{|p^0 - p^{0,H}|_{H^1(\Omega)}}_{e_{\mathrm{mac}}} + \underbrace{|p^{0,H} - p^H|_{H^1(\Omega)}}_{e_{\mathrm{mic}}} + \underbrace{|p^H - p^{H,\mathrm{RB}}|_{H^1(\Omega)}}_{e_{\mathrm{RB}}}. \tag{57}$$

Similarly to section 3.1, we can derive the following result.

Theorem 10. *If $p^0 \in H^{l+1}(\Omega)$, Assumtion **(Q)** holds, and $a^0(\cdot)$ is uniformly elliptic, bounded, and sufficiently smooth, then we have the following bound on the* macro error *$e_{\mathrm{mac}} \leq CH^l$, where the constant C is independent of H. The* micro error*, caused by discretiziation of micro problems, is bounded as*

$$e_{\mathrm{mic}} \leq C\|\mathbf{f}^H\|_{L^2(\Omega)} \max_{x\in Q^H} \|a^0(x) - a^{\mathcal{N}}(x)\|_F,$$

where C depends only on ellipticity and boundedness constants of $a^0(x)$ and $a^{\mathcal{N}}(x)$. The RB error e_{RB} is caused by using $a^{\mathrm{RB}}(x)$ instead of $a^{\mathcal{N}}$ in (16)*. We have*

$$e_{\mathrm{RB}} \leq C\|\mathbf{f}^H\|_{L^2(\Omega)} \max_{x\in Q^H} \|a^{\mathcal{N}}(x) - a^{\mathrm{RB}}(x)\|_F,$$

where C depends only on ellipticity and boundedness constants of $a^{\mathcal{N}}(x)$ and $a^{\mathrm{RB}}(x)$.

Proof. The proof is analogous to that of the a priori estimates of the DS-FE-HMM [2]. □

One can bound $\|a^0(x) - a^{\mathcal{N}}(x)\|_{\mathrm{F}}$ by the L_2 error of the micro solutions, which leads to

$$e_{\mathrm{mic}} \leq C\|\mathbf{f}^H\|_{L^2(\Omega)} \sum_{i=1}^{d} \|\mathbf{U}_{\mathrm{e}}^{i,x} - \mathbf{U}_{\mathcal{N}}^{i,x}\|_X \leq C\|\mathbf{f}^H\|_{L^2(\Omega)} \mathcal{N}^{-\frac{k+2}{d}}.$$

Such rate in $\mathcal{N}$ can be observed when micro meshes are adapted to the geometry (see section 8.1.1). Furthermore, under the assumptions from section 5.5 on the Kolomogorov n-width, we can obtain the a priori estimate $e_{\mathrm{RB}} \leq C\|\mathbf{f}^H\|_{L^2(\Omega)} e^{-cN_i^{\beta}}$.

6.2. A posteriori error estimates. Here we derive a posteriori error estimates that allow us to control the macro error e_{mac} and the RB error e_{RB}. The micro error in the RB framework comes from the discretization error of the micro problem (25). We recall that the number of degrees of freedom $\mathcal{N}$ for these problems is assumed to be large so that the offline computations of the RB solutions are very accurate. Hence, e_{mic} will be in general negligible.

Velocity reconstruction. We reconstruct a discontinuous velocity field using piecewise approximation of $a^{\mathrm{RB}}(\mathbf{f}^H - \nabla p^{H,\mathrm{RB}})$ by interpolation from quadrature points. In addition to the assumption **(Q)** we assume that the number of quadrature nodes J is minimal, i.e., $J = \binom{l+d-1}{d}$. Given a macro element $K \in \mathcal{T}_H$ and a function $q : Q^K \to \mathbb{R}$, there is a unique interpolant $\Pi(q) \in \mathcal{P}^{l-1}(K)$ such that $\Pi(q)(x_{K_j}) = q(x_{K_j})$ for every $j \in \{1, \ldots, J\}$ (see [30, Prop. 50], [8]). Therefore, for any tensor a defined on quadrature points x_{K_j}, there is a unique operator Π_a that maps $S^{l-1}_{\mathrm{dis},H}(\Omega)$ to itself (see (13)) and satisfies

$$\Pi_a(\mathbf{v})(x_{K_j}) = a(x)\mathbf{v}(x_{K_j}), \qquad \forall K \in \mathcal{T}_H, \quad \forall j \in \{1, \ldots, J\}.$$

We define the RB-DS-FE-HMM velocity reconstruction by $\mathbf{u}^{H,\mathrm{RB}} = \Pi_{a^{\mathrm{RB}}}(\mathbf{f}^H - \nabla p^{H,\mathrm{RB}})$.

Following the a posteriori error estimates in [2] we can define the *macro residual* η_K by

$$\begin{aligned}\eta_K^2 =& H_K^2 \|\nabla \cdot \Pi_{a^{\mathrm{RB}}}(\mathbf{f}^H - \nabla p^{H,\mathrm{RB}})\|^2_{L^2(K)} \\ &+ \textstyle\sum_{e\in\partial K} \frac{1}{2} H_e \|[\Pi_{a^{\mathrm{RB}}}(\mathbf{f}^H - \nabla p^{H,\mathrm{RB}}) \cdot \mathbf{n}]_e\|^2_{L^2(e)}\end{aligned}$$

for any $K \in \mathcal{T}_H$. The quantity η_K is computable and will serve as an error indicator. To state a rigorous a posteriori error estimate, we need to define additional (non-computable) errors:

the *RB error* $\xi_{\mathrm{RB},K}$, the *micro error* $\xi_{\mathrm{mic},K}$, and the *data approximation error* $\xi_{\mathrm{data},K}$ by

$$\xi_{\mathrm{RB},K}^2 = \|\mathbf{f}^H - \nabla p^{H,\mathrm{RB}}\|_{L^2(K)}^2 \max_{x\in Q^K} \|a^{\mathrm{RB}}(x) - a^{\mathcal{N}}(x)\|_{\mathrm{F}}^2,$$
$$\xi_{\mathrm{mic},K}^2 = \|\mathbf{f}^H - \nabla p^{H,\mathrm{RB}}\|_{L^2(K)}^2 \max_{x\in Q^K} \|a^{\mathcal{N}}(x) - a^{0}(x)\|_{\mathrm{F}}^2,$$
$$\xi_{\mathrm{data},K}^2 = \|a^0(\mathbf{f} - \nabla p^{H,\mathrm{RB}}) - \Pi_{a^0}(\mathbf{f}^H - \nabla p^{H,\mathrm{RB}})\|_{L^2(K)}^2.$$

Furthermore, for any quantity ξ_K that is defined for every $K \in \mathcal{T}_H$ let $\xi_M^2 = \sum_{K\in M} \xi_K^2$ for any $M \subset \mathcal{T}_H$. Finally, for any $K \in \mathcal{T}_H$ define $M(K)$ as the set of elements of $\mathcal{T}_H$ that share at least one edge with K. We then have the following theorem.

Theorem 11. *There is a constant C depending only on Ω, on the uniform continuity and coercivity constants of a^0 and on the shape-regularity of $\mathcal{T}_H$, such that*

$$|p^0 - p^{H,\mathrm{RB}}|_{H^1(\Omega)}^2 \le C \sum_{K\in\mathcal{T}_H} (\eta_K^2 + \xi_{\mathrm{RB},K}^2 + \xi_{\mathrm{mic},K}^2 + \xi_{\mathrm{data},K}^2).$$

Moreover, we have

$$\eta_K^2 \le C(|p^0 - p^{H,\mathrm{RB}}|_{H^1(M(K))}^2 + \xi_{\mathrm{RB},M(K)}^2 + \xi_{\mathrm{mic},M(K)}^2 + \xi_{\mathrm{data},M(K)}^2).$$

Proof. The proof is analogous to that in [2]. □

6.3. Assessment of the RB error. Even though we are not able to improve the RB precision in the online stage, we can assess the RB error online. Using (55) we have

$$\xi_{\mathrm{RB},K}^2 \le \|\mathbf{f}^H - p^{H,\mathrm{RB}}\|_{L^2(K)}^2 \max_{x\in Q^K} \Delta^{\mathrm{F}}(x) =: \eta_{\mathrm{RB},K}^2.$$

7 Adaptive method

We propose an adaptive RB-DS-FE-HMM that solves (16) by starting with a coarse macro mesh $\mathcal{T}_H$ that is successively refined based on the local error indicators η_K. The adaptive process follows the standard cycle SOLVE → ESTIMATE → MARK → REFINE.

Algorithm 12 (adaptive RB-DS-FE-HMM)**.** We assume that the offline RB stage is finished and the user provides Ω and an initial mesh $\mathcal{T}_H$.

1. *Solve.* For each quadrature point $x \in Q^H$ compute $a^{\mathrm{RB}}(x)$ using the online RB stage. Assemble and solve the macro elliptic problem (16).
2. *Estimate.* Compute η_K for every $K \in \mathcal{T}_H$.
3. *Mark.* Choose a subset of elements in $\mathcal{T}_H$ by using the error indicator η_K. We used the marking strategy E [44].
4. *Refine.* The marked elements are refined such that conformity and shape-regularity is preserved. The refined mesh stays denoted as $\mathcal{T}_H$.

The marking strategy contains one parameter that is usually denoted $\theta \in (0, 1)$. Smaller values of θ lead to more iteration steps but usually a better balancing of residuals (fewer outliers). Since the computation of a^{RB} is more expensive than solving the macro problem, we chose a relatively small value $\theta = 0.25$. Conformity and shape-regularity of the refined meshes is guaranteed by the newest vertex bisection method in two dimensions and by the modified longest edge bisection [11] in three dimensions.

For an efficient implementation of Algorithm 12 we save the tensors $a^{\mathrm{RB}}(x)$ for all quadrature points and new values of $a^{\mathrm{RB}}(x)$ are computed only in the refined elements. Further, one can check if the RB error is dominated by the macro error by computing $\eta_{\mathrm{RB},K}$ and comparing it to η_K.

8 Numerical Experiments

In this section we first validate the proposed RB method for Stokes micro problems. Second, we test the RB-DS-FE-HMM and compare it to the DS-FE-HMM [2]. Finally, we discuss the performance of the RB-DS-FE-HMM on a 3D problem.

On the macro scale, we will use $\mathcal{P}^1$, $\mathcal{P}^2$, or $\mathcal{P}^3$ elements. We only use the well-known Taylor-Hood $\mathcal{P}^2/\mathcal{P}^1$ elements on the micro scale (other stable FE pairs are of course possible).

Implementation. All experiments were performed on a single computer with two 8-core processors Intel Xeon E5-2600 and memory 8×8 GB DDR3 SDRAM 1600 MHz. The numerical codes were written in and run by Matlab R2014a with the startup option `-singleCompThread` that prohibits internal parallelization of Matlab. Some parts of the algorithm that are embarrassingly parallel were run using a `parfor` in a pool of 16 parallel single-threaded workers. For time measurement of a parallel job, we measure the execution time on each thread and sum the resulting times together. Hence, parallelizable parts can execute up to 16 times faster than the shown execution time.

The finite element code, inspired by [6, 20], uses vectorization to achieve fast assembling. Sparse linear systems for two-dimensional problems are solved by the Matlab routine `mldivide`. For three-dimensional systems we adopt the following strategy for the linear algebra:

- Positive definite systems are solved by the algebraic multigrid solver AGMG [31].
- Stokes systems are solved by the Uzawa method [33]. In the Uzawa method, AGMG was used as a preconditioner for the coercive part and the diagonal of the pressure mass matrix was used as a preconditioner of the Shur's complement.

Linear systems with the same positive definite matrix representing the scalar product on $X_{\mathcal{N}}$ are solved repeatedly in the offline algorithms[1]. We optimize this by precomputing a sparse Cholesky factorization (with reordering) provided by the Matlab routine `chol` and using it whenever we need to solve such system.

Eigenproblems and generalized eigenproblems from the SCM method were solved using the Matlab package `bleigifp` [35], which implements a block, inverse-free Krylov subspace method. Linear programming problems from the SCM method were run by the Matlab routine `linprog` with the default settings.

Micro mesh generation in DS-FE-HMM was done by external calls to `gmsh` [25].

8.1. Validation of the RB method. In this section we focus on the described RB method applied to micro problems and test its precision. Consider the two-dimensional micro geometry depicted in Figure 3, where the reference fluid part Y_{F} is L-shaped. Following Remark 2 we choose a square parametric domain $\mathcal{D} = (-0.2, 0.2)^2$ and consider the family of micro geometries $\{Y_{\mathrm{S}}^{\mu}, Y_{\mathrm{F}}^{\mu}\}_{\mu \in \mathcal{D}}$. The parametric domain $\mathcal{D}$ allows high variation of permeability but also avoids degenerate micro problems. In Figure 5 we plot the velocity solution of the micro problem in (5) for $i = 1$ and several different parameter values.

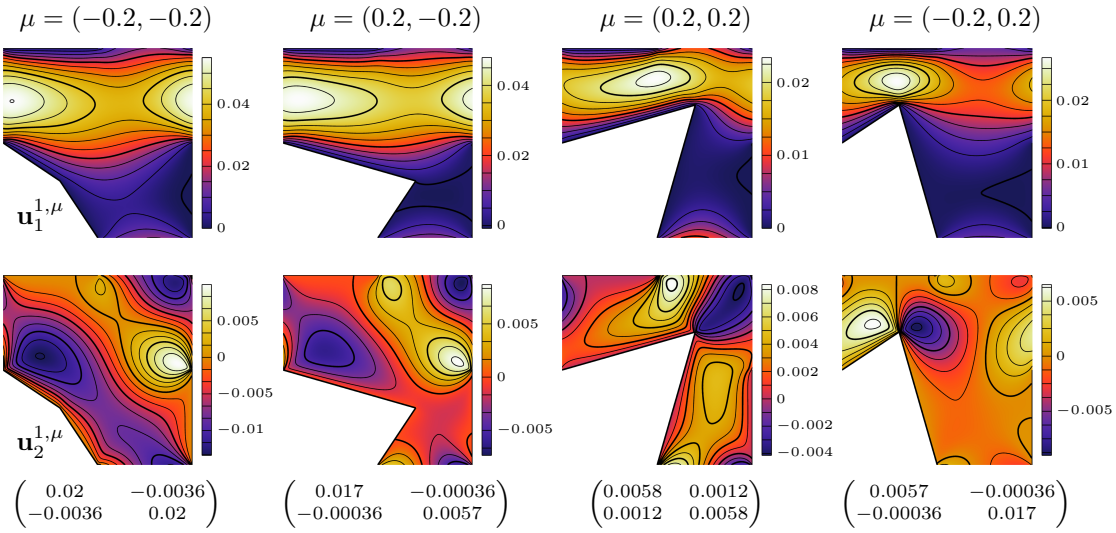

Figure 5: Velocity field $\mathbf{u}^{1,\mu} = (\mathbf{u}_1^{1,\mu}, \mathbf{u}_2^{1,\mu})$ of the micro problem (5) for $i = 1$ and for the four corner cases of parameter $\mu \in \mathcal{D}$ and approximate values of the corresponding tensors $a^0(\mu)$.

8.1.1. Reference micro meshes and discretization error. Usually, a fine mesh $\mathcal{T}_{\mathcal{N}}$ is defined in the reference domain Y_{F} and $\mathcal{T}_{\mathcal{N}}$ is assumed to be fine enough for the RB calculation so that the discretization error is negligible. For testing purposes, we consider a

[1] We solve these systems to compute supremizers in Algorithm 3 step 4 but also when solving the eigenproblems in Algorithm 5.

uniform meshes			graded meshes		
mesh	DOF ($\mathcal{N}$)	rel. err. (58)	mesh	DOF ($\mathcal{N}$)	rel. err. (58)
$\mathcal{T}_L^0$	126	$7.92 \cdot 10^{-2}$			
$\mathcal{T}_L^1$	470	$4.10 \cdot 10^{-2}$	$\mathcal{T}_{\text{ad}}^1$	478	$6.11 \cdot 10^{-2}$
$\mathcal{T}_L^2$	1806	$1.99 \cdot 10^{-2}$	$\mathcal{T}_{\text{ad}}^2$	1851	$6.07 \cdot 10^{-3}$
$\mathcal{T}_L^3$	7070	$9.50 \cdot 10^{-3}$	$\mathcal{T}_{\text{ad}}^3$	7265	$1.68 \cdot 10^{-4}$
$\mathcal{T}_L^4$	27966	$4.59 \cdot 10^{-3}$	$\mathcal{T}_{\text{ad}}^4$	28564	$1.32 \cdot 10^{-5}$
$\mathcal{T}_L^5$	111230	$2.23 \cdot 10^{-3}$	$\mathcal{T}_{\text{ad}}^5$	114893	$1.16 \cdot 10^{-6}$

Table 1: DOF and the relative discretization error (58) for different reference micro meshes: uniform ($\mathcal{T}_L^s$) and adaptive ($\mathcal{T}_{\text{ad}}^s$).

variety of meshes ranging from coarse to very fine and we asses the error originating from the RB discretization.

Let $\mathcal{T}_L^0$ be the coarse mesh of Y_{F} depicted in Figure 6(left). We define a family of meshes $\mathcal{T}_L^0, \mathcal{T}_L^1, \ldots$ such that $\mathcal{T}_L^s$ is obtained from $\mathcal{T}_L^{s-1}$ by a global uniform refinement as shown in Figure 6 (top).

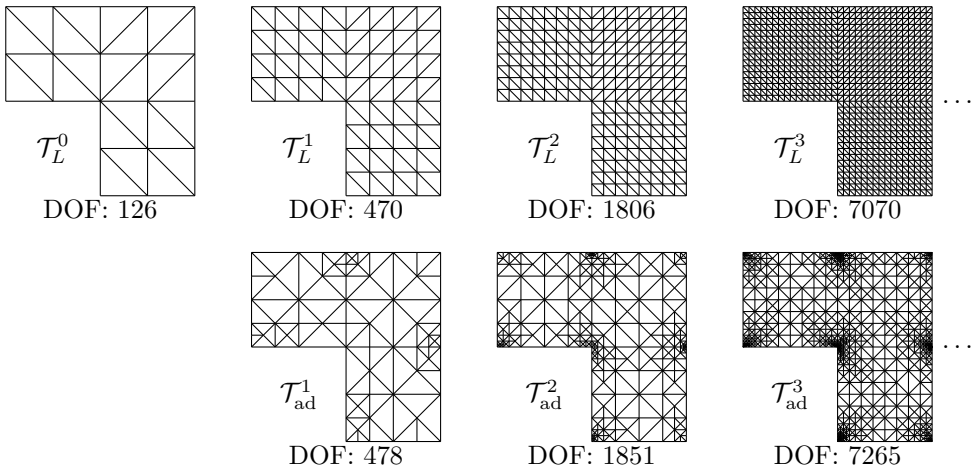

Figure 6: The three coarsest uniform meshes of the reference L-shaped micro domain Y_{F}.

We measure the discrepancy between the exact tensor $a^0(\mu)$ and the numerically computed tensor $a^{\mathcal{N}}(\mu)$ with the following numerical test. We select a uniform grid of parameters $\Xi_{\text{test}} \subset \mathcal{D}$ of size 17×17. Given a reference micro mesh $\mathcal{T}_L^s$, we compute $a^{\mathcal{N}}(\mu)$ for every $\mu \in \Xi_{\text{test}}$. Furthermore, we compute a precise approximation[2] of $a^0(\mu)$ for every $\mu \in \Xi_{\text{test}}$. Then we use the value

$$\max_{\mu \in \Xi_{\text{test}}} \frac{\|a^0(\mu) - a^{\mathcal{N}}(\mu)\|_{\text{F}}}{\|a^0(\mu)\|_{\text{F}}} \tag{58}$$

as an estimate of the maximal relative discretization error. The results of this experiment are shown in Table 1.

Since the micro domain is not convex, one expects that uniform meshes $\mathcal{T}_L^s$ are not optimal for the micro problem. A standard way to improve approximation properties of a mesh (when solving a single problem) is to use an adaptive method such as [43]. However, we aim for a mesh that would be fit not only for a single problem but a family of problems. We achieved very small discretization errors with micro meshes in the reference domain Y_{F} with the following approach. Starting with the coarse mesh $\mathcal{T} = \mathcal{T}_L^0$ we proceed with an iterative adaptive algorithm.

1. Map the mesh $\mathcal{T}$ to the domains Y_{F}^μ for the four corner parameters $\mu \in \mathcal{D}$, that is $\mu \in \{(-0.2, -0.2), (0.2, -0.2), (0.2, 0.2), (-0.2, 0.2)\}$.
2. In each of these *four* meshes we solve the *two* micro problems and compute the energy-based residuals (see [2, 43] for details).

[2] An approximation of the exact value $a^0(\mu)$ is computed for every $\mu \in \Xi_{\text{test}}$ just once by solving the micro problems in Y_{F}^μ with an adaptive FEM, where the stopping criteria were set to $5 \cdot 10^5$ DOF.

3. For each element in $\mathcal{T}$ we take the maximal residual over the eight problems and these values serve as residuals for marking and then refining the mesh $\mathcal{T}$ using the methods described in section 7.

We repeat these three steps until we reach the number of DOF of $\mathcal{T}_L^s$ for some $s \in \mathbb{N}$, when we denote the current refined mesh $\mathcal{T}$ by $\mathcal{T}_{\text{ad}}^s$. The meshes $\mathcal{T}_{\text{ad}}^s$ for $s \in \{1, 2, 3\}$ are shown in Figure 6. The discretization error of these meshes is shown in Table 1. It is clear from these computations that the adaptive meshes can give much better approximation of $a^0(\mu)$ with the same number of DOF as the uniform meshes.

8.1.2. SCM test. We next test the SCM Algorithm 5 with the different reference micro meshes from the previous subsection. The SCM involves several user-defined parameters, which were set as shown in Table 2.

The effectivity of the SCM is plotted in Figure 7, where we compared the estimated values $\beta_{\text{SCM}}(\mu)$ with numerically computed $\beta_{\text{Ba}}(\mu)$ for a fine grid of parameters $\mu \in \mathcal{D}$. For these SCM computations 120–180 eigenproblems and around $1.2 \cdot 10^6$ linear programming problems were solved.

parameter	value
tolerance ε_{SCM}	0.5
θ	0.5
training set size $N_{\text{train}}^{\text{SCM}}$	129×129
training set $\Xi_{\text{train}}^{\text{SCM}}$	regular grid in $\mathcal{D}$

Table 2: Parameters for the successive constraint method (SCM) used in Algorithm 5.

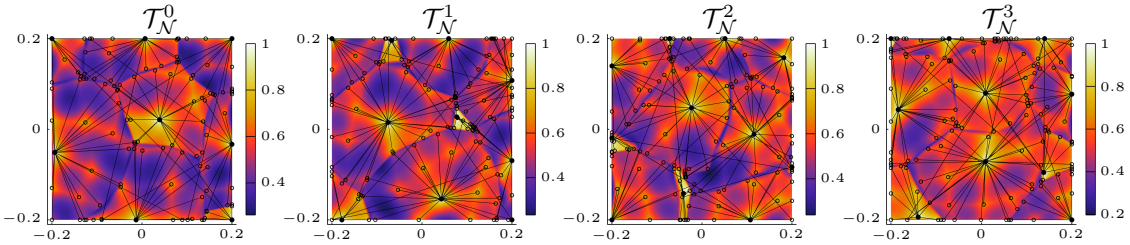

Figure 7: Effectivity of the proposed SCM Algorithm 5 for different $\mathcal{T}_{\mathcal{N}}$. The plots show the value $\beta_{\text{SCM}}(\mu)/\beta_{\text{Ba}}(\mu)$ for different $\mu \in \mathcal{D}$. Filled circles represent the values $\overline{\mu} \in S$ and they are connected to non-filled circles representing the points $C_{\overline{\mu}}$.

We note (see Table 3) that neither $|S|$ nor J increase with $\mathcal{N}$. However, the computational cost of solving the eigenproblems in the offline SCM increases with $\mathcal{N}$.

	$\mathcal{T}_L^3$	$\mathcal{T}_L^5$	$\mathcal{T}_{\text{ad}}^3$	$\mathcal{T}_{\text{ad}}^5$
$\lvert S\rvert$	10	10	11	11
J	103	112	119	118

Table 3: The sizes of the set S and the number $J = \sum_{\overline{x} \in S} |C_{\overline{x}}|$ in Algorithm 5 for different reference micro meshes.

8.1.3. RB Greedy test. We next test the greedy procedure of Algorithm 3 (assembling of the RB functions). The parameters were set according to Table 4. The desired tolerance was reached in $N_i \leq 70$ steps for $i = 1, 2$ for all tested micro meshes. The convergence of the greedy algorithm is plotted in Figure 8 and it appears to be exponential in N_i. The indicator of the error in the output of interest $\Delta^{\text{F}}(x)$ (see (55)) is quadratic with respect to the indicators of the error of the solution $\Delta_i^{\text{E}}(x)$ (see (43)). We note that the round-off error can become an issue for very small residuals, which is addressed in [19].

8.2. Validation of the RB-DS-FE-HMM. In this section we validate the RB-DS-FE-HMM and see how different sources of errors (macro, micro, RB) influence the total error. We choose a 2D experiment based on the micro geometries and meshes that were tested in the previous section. Let $\Omega \subset \mathbb{R}^2$ be a piecewise polygonal domain as depicted in Figure 4(right)

parameter	value
tolerance $\varepsilon_{\mathrm{RB}}$	10^{-5}
training set size $N_{\mathrm{train}}^{\mathrm{RB}}$	65×65
training set $\Xi_{\mathrm{train}}^{\mathrm{RB}}$	regular grid in $\mathcal{D}$

Table 4: Parameters for the greedy RB construction used in Algorithm 3.

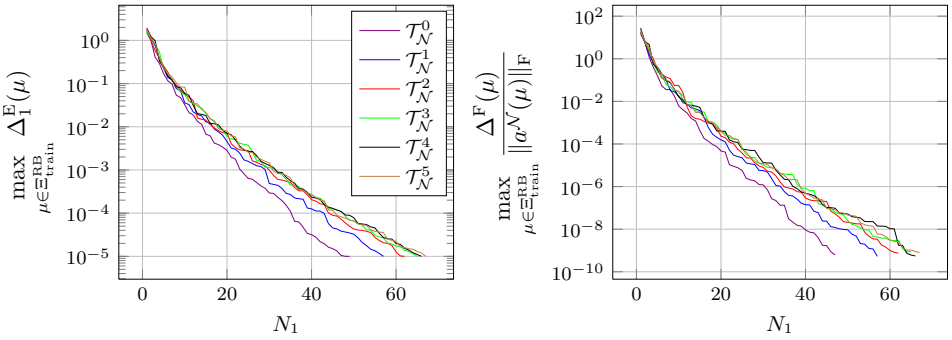

Figure 8: Greedy Algorithm 3 in practice: decreasing tendency of the maximal residual for the first micro problem for four different $\mathcal{N}$.

with $\mathcal{T}_H$ as an initial mesh and let us define a porous structure in Ω with geometries from Figure (3) and $\mu : \Omega \to \mathcal{D}$ given by

$$\mu(x) = \left(\frac{1}{5} \cos\left(\frac{\pi(x_2 - x_1)}{2} \right), \frac{1}{5} \cos\left(\frac{\pi(x_2 + x_1)}{2} \right) \right) \in \mathcal{D}. \tag{59}$$

We assume that the force field is constant $\mathbf{f} \equiv (0, -1)$ and that the edges $(0, 2) \times \{0\}$ and $(0, 2) \times \{4\}$ in the macroscopic domain Ω are connected periodically. The homogenized solution p^0 and non-homogenized solutions of (1) are shown in Figure 9.

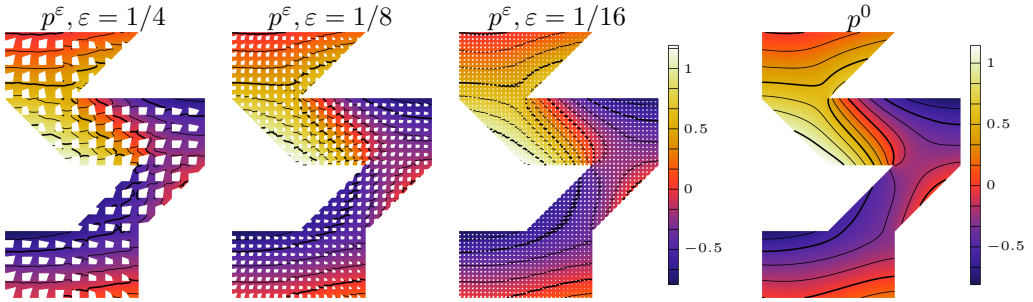

Figure 9: Pressure solutions p^ε to (1) for varying size of $\varepsilon > 0$ (left). Homogenized solution p^0 to (2) (right).

We next run the RB-DS-FE-HMM with different settings (macro FE, number of RB functions N_i, micro mesh) to detail the error behavior. We stop the adaptive method when the number of macro degrees of freedom (N_{mac}) reaches 10^4.

Remark 13. Since we do not have an analytic reference solutions, all the errors from the error decomposition (57) are only estimated as follows. We compute approximations to p^H, $p^{0,H}$, p^0, which are denoted by $\tilde{p}^H$, $\tilde{p}^{0,H}$, $\tilde{p}^0$, respectively, and substitute them into (57) to get approximations of e_{mac}, e_{mic}, and e_{RB}.

- $\tilde{p}^H$ is a solution obtained from the RB-DS-FE-HMM with the complete RB (setting N_i to the maximum) but with the same macro mesh and micro reference mesh as $p^{H,\mathrm{RB}}$.
- $\tilde{p}^{0,H}$ is a solution obtained from the RB-DS-FE-HMM with the complete RB (setting N_i to the maximum), the same macro mesh as $p^{H,\mathrm{RB}}$, and the finest micro mesh $\mathcal{T}_{\mathrm{ad}}^5$.
- $\tilde{p}^0$ is a solution obtained from the RB-DS-FE-HMM with the complete RB (setting N_i to the maximum), the finest micro mesh $\mathcal{T}_{\mathrm{ad}}^5$, and the macro mesh obtained by two uniform refinements of the macro mesh used for the finest solution $p^{H,\mathrm{RB}}$.

Coarse micro mesh and small RB. We first illustrate what happens if a coarse micro mesh is taken. Let us use the mesh $\mathcal{T}_{\mathcal{N}}^0$ for micro problems. We take only three RB functions ($N_1 = N_2 = 3$) generated by the greedy algorithm.

We run the adaptive RB-DS-FE-HMM with two different macro FE: $\mathcal{P}^1$ and $\mathcal{P}^3$. The results are depicted in Figure (10). We see that the micro error e_{mic} becomes soon dominant and is the main reason for saturation of the global error $e = |p^0 - p^{H,\text{RB}}|_{H^1(\Omega)}$.

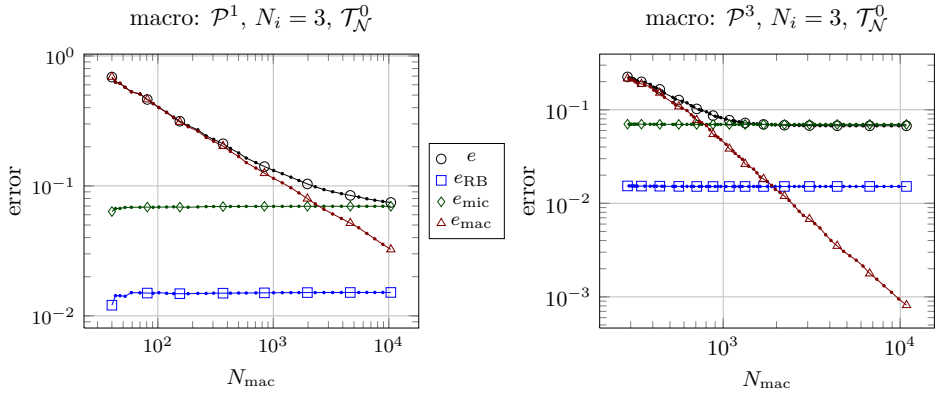

Figure 10: Error plot of the adaptive RB-DS-FE-HMM: 3 RB functions ($N_1 = N_2 = 3$) and the coarse micro mesh $\mathcal{T}_{\mathcal{N}}^0$.

Fine uniform micro mesh and small RB. In the next experiment we keep 3 RB functions but take the most refined uniform micro mesh $\mathcal{T}_{\mathcal{N}}^5$. As before, we run the experiment for $\mathcal{P}^1$ and $\mathcal{P}^3$ macro elements and the error rates are plotted in Figure 11. The micro error e_{mic} is now dominated by the RB error e_{RB}. For $\mathcal{P}^3$ macro FE the RB error causes the saturation of the global error e for $N_{\text{mac}} > 10^3$.

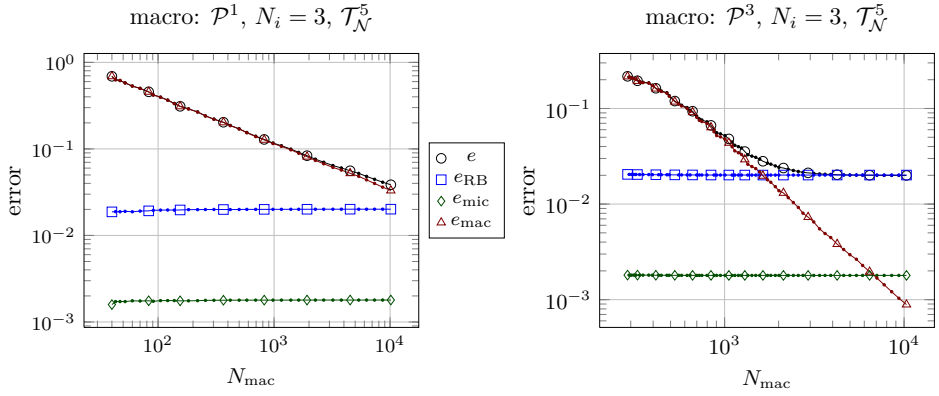

Figure 11: Error plot of the adaptive RB-DS-FE-HMM: 3 RB functions ($N_1 = N_2 = 3$) and fine uniform micro meshes $\mathcal{T}_{\mathcal{N}}^5$.

Fine uniform micro mesh and a larger RB. We now increase the number of RB functions to 10 and repeat the experiment with the most refined uniform micro mesh $\mathcal{T}_{\mathcal{N}}^5$. The experiments for $\mathcal{P}^1$ and $\mathcal{P}^3$ macro FE are depicted in Figure 12. We see that the RB error e_{RB} is negligible compared to the other errors for N_{mac} up to 10^4. However, for $\mathcal{P}^3$ macro FE we see a saturation of the global error close to 10^4 DOF due to the micro error.

Graded micro mesh and a larger RB. We now show the advantage of a graded micro mesh over the uniform micro meshes. We use the graded mesh $\mathcal{T}_{\mathcal{N}}^{\text{ad},3}$, which has approximately 16 times less DOF than $\mathcal{T}_{\mathcal{N}}^5$, and we keep 10 RB functions as in the previous experiment. We use $\mathcal{P}^3$ macro FEs and stop the adaptive RB-DS-FE-HMM when we reach 10^4 macro DOF. The convergence rates are depicted in Figure 13. The micro error is approximately 10 times smaller with 16 times less DOF on micro scale. The global error saturation is not visible in the figure and happens only after one reaches more than $2 \cdot 10^4$ DOF.

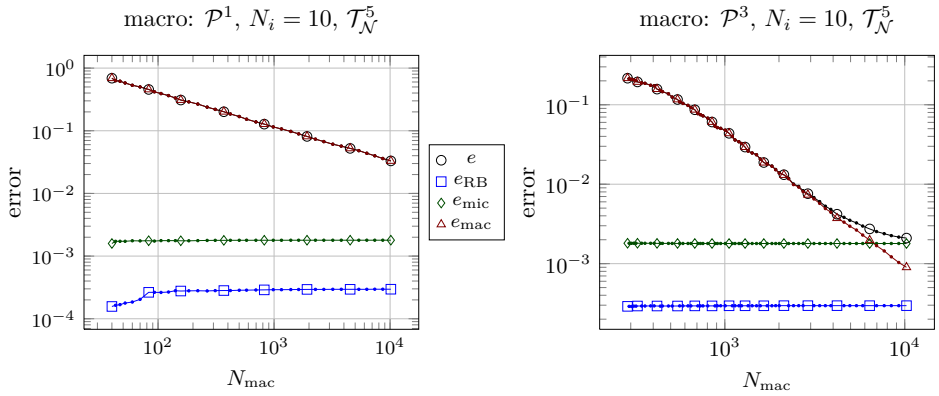

Figure 12: Error plot of the adaptive RB-DS-FE-HMM: 10 RB functions ($N_1 = N_2 = 10$) and fine uniform micro meshes $\mathcal{T}_{\mathcal{N}}^5$.

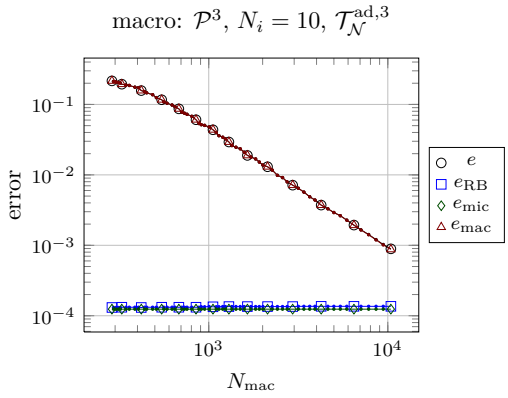

Figure 13: Error plot of the adaptive RB-DS-FE-HMM: 10 RB functions ($N_1 = N_2 = 10$) and graded micro meshes $\mathcal{T}_{\mathcal{N}}^{\text{ad},3}$.

8.3. Performance comparison: RB-DS-FE-HMM vs. DS-FE-HMM. In this subsection we compare the performance of the RB-DS-FE-HMM and the DS-FE-HMM (see [2]) on the problem from the previous subsection. We keep the macro domain Ω and the initial macro mesh $\mathcal{T}_H$. The micro geometries are as in Figure 3 and their variation is described by (59). The force field $\mathbf{f}$ has a constant value $(0, -1)$ and we use $\mathcal{P}^2/\mathcal{P}^1$ Taylor-Hood elements on the micro scale. We use adaptive mesh refinement for both methods and use the same marking scheme with $\theta = 0.25$ on macro scale.

Offline stage. The DS-FE-HMM is an offline/online method, where constants for the calibration of the adaptive process are precomputed in the offline stage [2]. This precomputation took 3380 s. The offline stage of the RB-DS-FE-HMM depends on many parameters, however, we decided to fix the tolerance and sampling parameters as in Table 2 and Table 4. We plot the offline CPU time in Table 5 for some selected micro meshes.

A careful inspection of Table 5 reveals that the most costly part in the current implementation is the SCM. Both the offline part of Algorithm 5 and the evaluation of SCM lower bounds in Algorithm 3 are very costly. However, excluding the SCM part, Algorithm 3 appears to be quite efficient, compared to the DS-FE-HMM preprocessing.

Online stage. We further provide a comparison of the main computation. Performance of the online RB-DS-FE-HMM does not depend significantly on the used micro mesh, hence we chose $\mathcal{T}_{\mathcal{N}}^5$. We performed the adaptive methods and stopped after the number of macro DOF reached 10^2, 10^3, and 10^4. The pairs of solutions from the two methods have very similar accuracy since the macroscopic error is dominating. See Table 6 for the comparison.

8.4. A 2D experiment with more complex geometry. In this subsection we apply RB-DS-FE-HMM to another 2D problem with a more complex micro and macro ge-

RB-DS-FE-HMM offline CPU time [s]		mesh			
part	subpart	$\mathcal{T}_L^3$	$\mathcal{T}_L^5$	$\mathcal{T}_{\text{ad}}^3$	$\mathcal{T}_{\text{ad}}^5$
SCM	eigenproblems	480	38948	402	21509
Algorithm 5	linear programming	8913	8566	9610	9477
RB greedy	assembling	5	133	6	129
Algorithm 3	fine solve (Stokes)	23	621	24	350
	fine solve (supremizers)	2	85	2	43
	residuals (without SCM)	30	31	37	31
	SCM for residuals	567	585	641	628

Table 5: Offline CPU time for the RB-DS-FE-HMM with different micro meshes. Settings in Table 2 and Table 4, with $Q_A = 15$, $Q = 3$.

DS-FE-HMM online stage			RB-DS-FE-HMM online stage			
					$N_i = 10$	$N_i = 89$
iteration	DOF	CPU time(s)	iteration	DOF	CPU time(s)	
10	113	244	9	106	6	7
24	1116	4500	24	1158	19	56
38	11372	179724	37	10151	63	733

Table 6: Online CPU time of the adaptive methods. We compare solutions after reaching 10^2, 10^3, and 10^4 macroscopic degrees of freedom.

ometries. The macro geometry with the initial macro mesh $\mathcal{T}_H$ is depicted in Figure 15(left). We use periodic boundary conditions over the boundary edges $(1,2) \times \{0\}$ and $(1,2) \times \{4\}$ and assume the force field $\mathbf{f} \equiv (0,-1)$. We set $\mathcal{D} = (-1/12, 1/12) \times (-1/12, 1/12)$. The reference micro domain and the mesh of its fluid part is sketched in Figure 14. Micro geometry variations with respect to a two dimensional parameter $\mu \in \mathcal{D}$ is depicted in Figure 15. The micro cell Y is divided into 3×3 grid, whose tiles are affinely deformed by $\varphi(\mu, \cdot)$. The dependence of $\mu \in \mathcal{D}$ on $x \in \Omega$ is governed by the function

$$\mu(x) = (\ \cos(2\pi(x_2 - x_1)/4)/12,\ \cos(2\pi(x_2 + x_1)/4)/12\ ).$$

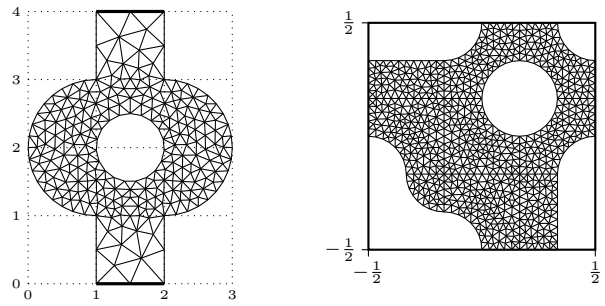

Figure 14: Experiment from section 8.4. Initial macro mesh with periodic BC indicated by thick lines (left) and the reference micro mesh (right).

The variation of the micro geometry is visible in Figure 16(left), where the original (non-homogenized) pressure solutions are plotted. We observe that with decreasing ε the pressure solutions agree with the homogenized solution in Figure 16(right).

The affine decomposition in this case resulted to $Q_A = 12$ and $Q = 4$ and the number of DOF of the micro problems is equal to 6752. In the offline RB stage we used the same settings as before, see Table 2 and Table 4. Reaching the required tolerance in Algorithm 3 yields $N_1 = N_2 = 44$ RB functions.

We run the RB-DS-FE-HMM with only $N_1 = N_2 = 15$ RB functions, which still yields the RB error to smaller than the micro error. The convergence rates with respect to macro DOF are as expected and plotted in Figure 17(left), where saturation of the error can be observed. We repeated the same experiment but with once uniformly refined micro reference mesh and the convergence rates indeed improved, see Figure 17(right).

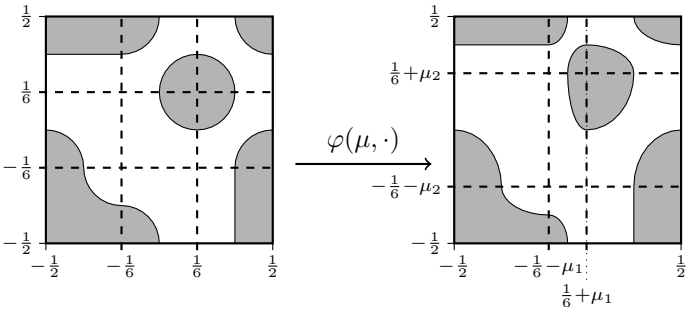

Figure 15: Experiment from section 8.4. Transformation $\varphi(\mu,\cdot)$ that maps the reference micro geometry (left) to a local geometry (right) for any $\mu \in \mathcal{D}$.

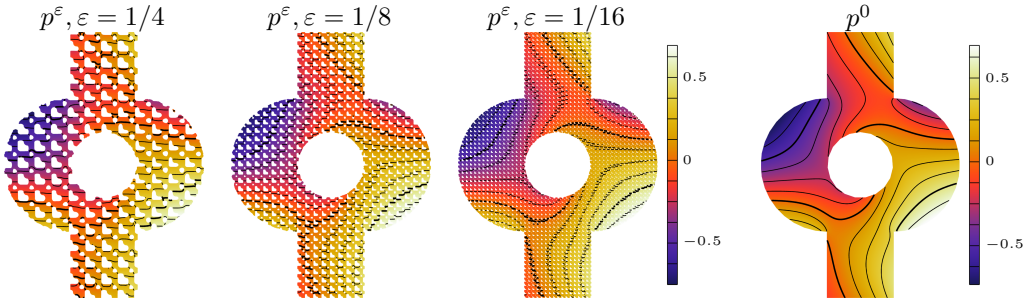

Figure 16: Pressure solutions p^ε to (1) for varying size of $\varepsilon > 0$ (left). Homogenized solution p^0 to (2) (right).

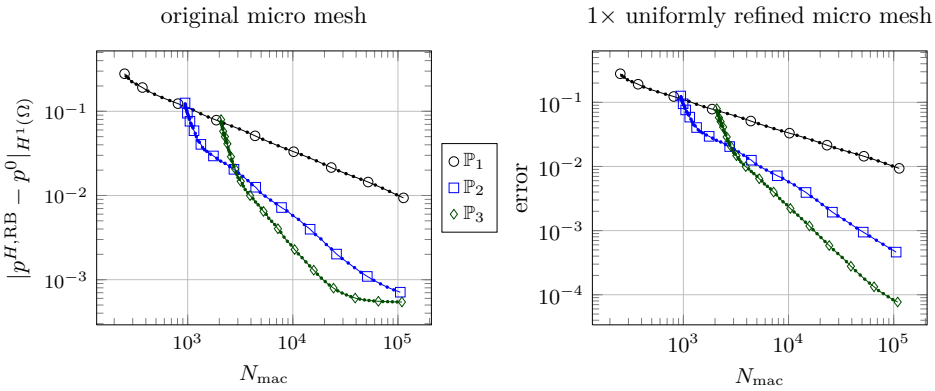

Figure 17: RB-DS-FE-HMM convergence rates for the experiment from section 8.4 with different macro elements (left). The same with finer (once uniformly refined) micro reference mesh (right).

8.5. A 3D experiment. In this subsection we present a 3D experiment. The macro geometry is a geometrical extrusion of the 2D macro geometry from section 8.4 and is depicted in Figure 18(left). The coarse macro mesh $\mathcal{T}_H$ with 7152 elements and 1605 nodes is plotted in Figure 18(right). We keep the structure of the previous problems and define periodic boundary conditions between the faces $(1,2)\times(0,1)\times\{0\}$ and $(1,2)\times(0,1)\times\{4\}$. Furthermore, we assume a constant force field $\mathbf{f} \equiv (0,0,-1)$.

The porous structure in Ω is given as follows. We set $\mathcal{D} = (-1/12, 1/12)^3$. The reference micro geometry and its variation with respect to a three dimensional parameter $\mu \in \mathcal{D}$ is depicted in Figure 19. The micro cell Y is divided into 3×3 grid whose tiles are dilated in coordinate directions, depending on the parameter. The dependence of $\mu \in \mathcal{D}$ on $x \in \Omega$ is

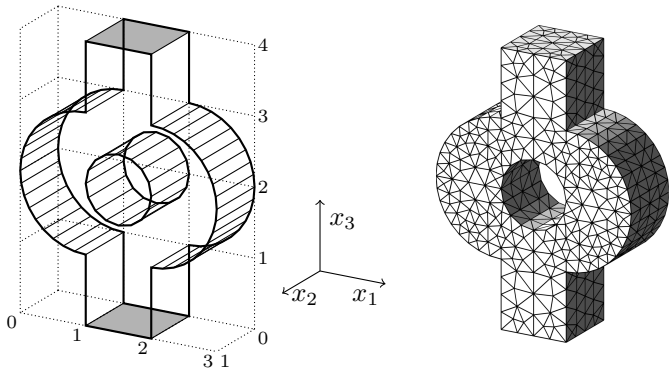

Figure 18: Three-dimensional macro geometry with periodic faces in gray (left) and a the coarse mesh (right).

governed by the function

$$\begin{aligned}\mu(x) = (\,&\cos(\pi(-x_1 + x_2 - x_3)/2)/12,\\ &\cos(\pi(-x_1 + x_2 + x_3)/2)/12,\\ &\cos(\pi(x_1 + x_2 + x_3)/2)/12).\end{aligned}$$

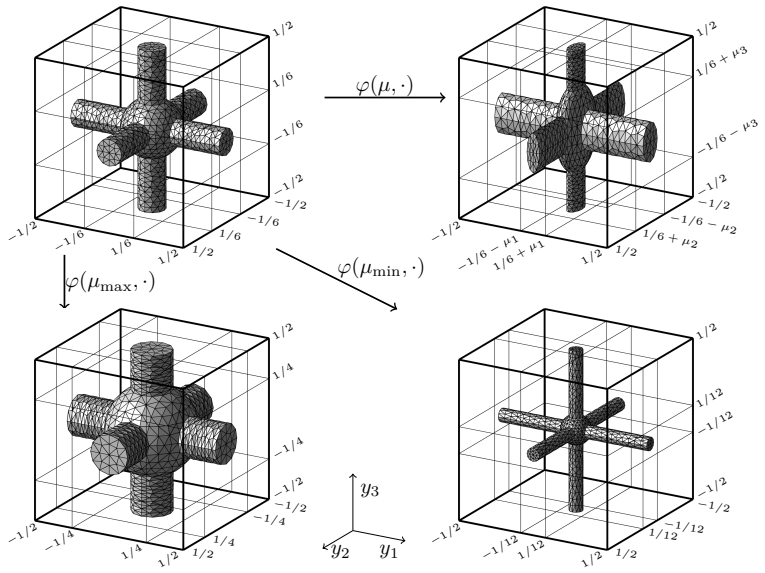

Figure 19: Three-dimensional micro reference mesh (above left) and some mapped micro domains Y_{F}^{μ} with $\mu = (-1/12, 0, 1/12)$ (above right), $\mu_{\max} = (1/12, 1/12, 1/12)$ (bottom left) and $\mu_{\min} = (-1/12, -1/12, -1/12)$ (bottom right).

We performed the RB-DS-FE-HMM experiment with $\mathcal{P}^1$ macro elements and $N_1 = N_2 = N_3 = 10$. We reached the expected convergence rate of $N_{\mathrm{mac}}^{-1/3}$, as is depicted in Figure 20.

Several additional challenges arise for such a large 3D experiment. The main problem is that the Cholesky factorization of the scalar product matrix can be too expensive to compute and store, when computing a fine reference micro RB problem. We resolved this by running the AGMG solver to compute each supremizer in Algorithm 3. Furthermore, the SCM also relies on the Cholesky factorization even more (used in 2D in each eigenproblem at each iteration). There are various ways to address this problem:

- Apply the SCM for a coarser micro mesh than used for computing the micro functions.
- Compute $\beta_{\mathrm{Ba}}^{\mathcal{N}}(x)$ on a coarse grid in Ω and define $\beta_{\mathrm{SCM}}^{\mathcal{N}}(x)$ for any $x \in \Omega$ by a linear interpolation over the grid.
- Set a constant inf-sup estimate $\beta_{\mathrm{SCM}}^{\mathcal{N}}(x) \equiv \beta_{\mathrm{Ba}}^{\mathcal{N}}(x_{\mathrm{ref}})$.

While none of these approaches guarantee $\beta_{\mathrm{Ba}}^{\mathcal{N}}(x) \geq \beta_{\mathrm{SCM}}^{\mathcal{N}}(x)$, they can perform quite well

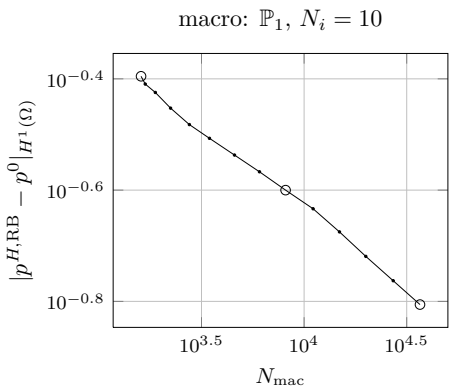

Figure 20: Convergence rates of the RB-DS-FE-HMM algorithm for the 3D experiment.

in practice if the function $\beta^{\mathcal{N}}_{\mathrm{Ba}}(x)$ is smooth and with small relative variance. In the 3D experiment we used the second approximation method for the SCM of the test problem.

9 Conclusion

We have presented an efficient multiscale FE method for the Stokes flow in porous media. In our new method, the RB-DS-FE-HMM, we avoid the repeated direct solution of Stokes micro problems at each macro quadrature point, which is the main bottleneck of the DS-FE-HMM. Instead, we map the micro problems into a reference domain and construct a Petrov-Galerkin reduced basis method for their solutions. With a greedy alorithm we select a small number of micro problems that are solved on a reference micro mesh. Then, a RB interpolation is used to obtain a cheap and accurate estimate of the effective permeability for any parameter (macro quadrature point). We have discussed an a posteriori error estimate for the selection of representative micro solutions including the estimation of the (inf-sup) stability constant. We have derived an a priori and a posteriori error analysis of the multiscale method, which lead to an adaptive method for the macro discretization. The accuracy, versatility, and efficiency of the RB-DS-FE-HMM has been illustrated by several numerical examples. Comparisons with the DS-FE-HMM have shown significant speedup in the online stage of the methods.

References

[1] Abdulle, A. A priori and a posteriori error analysis for numerical homogenization: a unified framework. *Ser. Contemp. Appl. Math. CAM 16* (2011), 280–305.

[2] Abdulle, A., and Budáč, O. An adaptive finite element heterogeneous multiscale method for Stokes flow in porous media. *Multiscale Model. Simul. 13* (2015), 256–290.

[3] Abdulle, A., and Budáč, O. Multiscale adaptive method for Stokes flow in heterogenenous media. In *Numerical Mathematics and Advanced Applications - ENUMATH 2013*, Lect. Notes Comput. Sci. Eng. Springer, 2015, pp. 367–375.

[4] Abdulle, A., and Budáč, O. A Petrov–Galerkin reduced basis approximation of the Stokes equation in parameterized geometries. *C. R. Math. Acad. Sci. Paris 353*, 7 (2015), 641–645.

[5] Abdulle, A., E, W., Engquist, B., and Vanden-Eijnden, E. The heterogeneous multiscale method. *Acta Numer. 21* (2012), 1–87.

[6] Abdulle, A., and Nonnenmacher, A. A short and versatile finite element multiscale code for homogenization problems. *Comput. Methods Appl. Mech. Engrg. 198*, 37–40 (2009), 2839–2859.

[7] Abdulle, A., and Nonnenmacher, A. Adaptive finite element heterogeneous multiscale method for homogenization problems. *Comput. Methods Appl. Mech. Engrg. 200*, 37–40 (2011), 2710–2726.

[8] Abdulle, A., and Nonnenmacher, A. A posteriori error estimates in quantities of interest for the finite element heterogeneous multiscale method. *Numer. Methods Partial Differential Equations 29*, 5 (2013), 1629–1656.

[9] Allaire, G. Homogenization of the Stokes flow in a connected porous medium. *Asymptot. Anal. 2*, 3 (1989), 203–222.

[10] Alyaev, S., Keilegavlen, E., and Nordbotten, J. M. Analysis of control volume heterogeneous multiscale methods for single phase flow in porous media. *Multiscale Model. Simul. 12*, 1 (2014), 335–363.

[11] Arnold, D. N., Mukherjee, A., and Pouly, L. Locally adapted tetrahedral meshes using bisection. *SIAM J. Sci. Comput. 22*, 2 (2000), 431–448.

[12] Babuška, I. The finite element method with Lagrangian multipliers. *Numer. Math. 20*, 3 (1973), 179–192.

[13] Barrault, M., Maday, Y., Nguyen, N.-C., and Patera, A. T. An 'empirical interpolation method': Application to efficient reduced-basis discretization of partial differential equations. *C. R. Math. Acad. Sci. Paris Ser.I 339* (2004), 667–672.

[14] Beliaev, A. Y., and Kozlov, S. M. Darcy equation for random porous media. *Comm. Pure Appl. Math. 49*, 1 (1996), 1–34.

[15] Binev, P., Cohen, A., Dahmen, W., Devore, R., Petrova, G., and Wojtaszczyk, P. Convergence rates for greedy algorithms in reduced basis methods. *SIAM J. Math. Anal. 43* (2011), 1457–1472.

[16] Boffi, D., Brezzi, F., and Fortin, M. Finite elements for the Stokes problem. In *Mixed Finite Elements, Compatibility Conditions, and Applications*. Springer, 2008, pp. 45–100.

[17] Brezzi, F. On the existence, uniqueness and approximation of saddle-point problems arising from Lagrangian multipliers. *ESAIM Math. Model. Numer. Anal. 8*, R2 (1974), 129–151.

[18] Brown, D. L., Efendiev, Y., and Hoang, V. H. An efficient hierarchical multiscale finite element method for Stokes equations in slowly varying media. *Multiscale Model. Simul. 11*, 1 (2013), 30–58.

[19] Casenave, F. Accurate a posteriori error evaluation in the reduced basis method. *§C. R. Math. Acad. Sci. Paris 350*, 9 (2012), 539–542.

[20] Chen, L., and Zhang, C.-S. AFEM@Matlab: a matlab package of adaptive finite element methods. Tech. rep., Department of Mathematics, University of Maryland at College Park, 2006.

[21] Ciarlet, P. G. *The finite element method for elliptic problems*, vol. 4 of *Studies in Mathematics and its Applications*. North-Holland, 1978.

[22] Dahmen, W., Plesken, C., and Welper, G. Double greedy algorithms: reduced basis methods for transport dominated problems. *M2AN Math. Model. Numer. Anal. 48*, 03 (2014), 623–663.

[23] Demkowicz, L. Babuška ↔ Brezzi. Tech. rep., Texas Institute for Computational and Applied Mathematics, The University of Texas at Austin, 2006.

[24] Gerner, A.-L., and Veroy, K. Certified reduced basis methods for parametrized saddle point problems. *SIAM J. Sci. Comput. 34*, 5 (2012), A2812–A2836.

[25] Geuzaine, C., and Remacle, J.-F. Gmsh: A three-dimensional finite element mesh generator with built-in pre- and post-processing facilities. *Internat. J. Numer. Methods Engrg. 79*, 11 (2009), 1309–1331.

[26] Huynh, D. B. P., Knezevic, D. J., Chen, Y., Hesthaven, J. S., and Patera, A. T. A natural-norm successive constraint method for inf-sup lower bounds. *Comput. Methods Appl. Mech. Engrg. 199*, 29 (2010), 1963–1975.

[27] Maday, Y., Patera, A. T., and Rovas, D. V. A blackbox reduced-basis output bound method for noncoercive linear problems. In *Nonlinear partial differential equations and their applications. Collège de France Seminar*, vol. 31. North-Holland, 2001, pp. 533–569.

[28] Marušić-Paloka, E., and Mikelić, A. An error estimate for correctors in the

homogenization of the Stokes and Navier-Stokes equations in a porous medium. *Boll. Unione Mat. Ital. 10*, 3 (1996), 661–671.

[29] Mikelić, A. *Homogenization theory and applications to filtration through porous media.* Springer, 2000, pp. 127–214.

[30] Nonnenmacher, A. *Adaptive Finite Element Methods for Multiscale Partial Differential Equations.* PhD thesis, École Polytechnique Fédérale de Lausanne, 2011.

[31] Notay, Y. An aggregation-based algebraic multigrid method. *Electron. Trans. Numer. Anal. 37*, 6 (2010), 123–146.

[32] Ohlberger, M. A posteriori error estimates for the heterogeneous multiscale finite element method for elliptic homogenization problems. *Multiscale Model. Simul. 4*, 1 (2005), 88–114.

[33] Peters, J., Reichelt, V., and Reusken, A. Fast iterative solvers for discrete Stokes equations. *SIAM J. Sci. Comput. 27*, 2 (2005), 646–666.

[34] Pierce, N. A., and Giles, M. B. Adjoint recovery of superconvergent functionals from PDE approximations. *SIAM Rev. 42*, 2 (2000), 247–264.

[35] Quillen, P. D. *Generalizations of an inverse free Krylov subspace method for the symmetric generalized eigenvalue problem.* PhD thesis, University of Kentucky, 2005.

[36] Rovas, D. V. *Reduced-basis output bound methods for parametrized partial differential equations.* PhD thesis, Massachusetts Institute of Technology, 2003.

[37] Rozza, G., Huynh, D. B. P., and Manzoni, A. Reduced basis approximation and a posteriori error estimation for Stokes flows in parametrized geometries: roles of the inf-sup stability constants. *Numer. Math. 125*, 1 (2013), 1–38.

[38] Rozza, G., Huynh, D. B. P., and Patera, A. T. Reduced basis approximation and a posteriori error estimation for affinely parametrized elliptic coercive partial differential equations. *Arch. Comput. Methods. Eng. 15* (2008), 229–275.

[39] Rozza, G., and Veroy, K. On the stability of the reduced basis method for Stokes equations in parametrized domains. *Comput. Methods Appl. Mech. Engrg. 196*, 7 (2007), 1244–1260.

[40] Sánchez-Palencia, E. *Non-homogeneous media and vibration theory*, vol. 127 of *Lecture Notes in Phys.* Springer, 1980.

[41] Sandström, C., Larsson, F., Runesson, K., and Johansson, H. A two-scale finite element formulation of Stokes flow in porous media. *Comput. Methods Appl. Mech. Engrg. 261–262* (2013), 96–104.

[42] Tartar, L. *Incompressible fluid flow in a porous medium—convergence of the homogenization process.* Vol. 127 of *Lecture Notes in Phys.* [40], 1979, ch. Appendix, pp. 368–377.

[43] Verfürth, R. A posteriori error estimators for the Stokes equations. *Numer. Math. 55*, 3 (1989), 309–325.

[44] Verfürth, R. *A review of a posteriori error estimation and adaptive mesh-refinement techniques.* Wiley-Teubner, New-York, 1996.

[45] Xu, J., and Zikatanov, L. Some observations on Babuška and Brezzi theories. *Numer. Math. 94*, 1 (2003), 195–202.